Bachelor's Thesis

Thermophoretic Behaviour of UV-Damaged CPD vs. Undamaged TT-dimers under Nonequilibrium Conditions

Department of Physics
Ludwig-Maximilians-Universität München

Benjamin Ebert

Munich, December 4th, 2024

Submitted in partial fulfillment of the requirements for the degree of B. Sc.
Supervised by Paula Aikkila, Prof. Dr. Dieter Braun

Bachelorarbeit

Thermophoretisches Verhalten von UV-geschädigten CPD vs. unbeschädigten TT-Dimeren unter Nicht-Gleichgewichtsbedingungen

Fakultät für Physik
Ludwig-Maximilians-Universität München

Benjamin Ebert

München, 4. Dezember 2024

Eingereicht im Rahmen der Anforderungen für den Abschluss des Studiengangs Bachelor of Science.
Betreuung: Paula Aikkila, Prof. Dr. Dieter Braun

Abstract

In a vertically oriented chamber with a temperature gradient, thermophoretic and convective forces drive circulating currents. These currents accumulate dissolved substances at varying concentrations and heights, influenced by their thermophoretic properties. These properties are expressed by the Soret coefficient, which is given by the environmental conditions and the substance's molecular structure. The accumulation of genetic material in a localized area is significant because it increases the likelihood of polymerization, facilitating the formation of longer DNA or RNA chains. In this work, which is affiliated to the field of research called "Origins of Life", the change in the thermophoretic behavior of thymine dimers has been studied, after they have been mutated into cyclobutane pyrimidine dimers (CPDs), the most common type of photodamage. The CPDs were created using a method called photosensitizing, with acetone serving as the medium to facilitate the formation of photodamage through UV irradiation. The damaged and undamaged DNA samples were then mixed and placed in a gravitational thermal trap for several hours before being analyzed. The results indicate that CPD-DNA accumulates more in the lower part of the chamber, suggesting it has a higher Soret coefficient compared to undamaged DNA.

Contents

1 Introduction

The blueprints for constructing the body of a living organism are stored within its DNA or RNA. They are the foundation of the mechanisms in a fully evolved organism, enabling abilities like growth, self-repair and replication. Life as we know it has existed and matured for millions of years. But how did it begin? A interdisciplinary group of scientists is approaching this questions within this field of research called "Origins of life".

One hypothesis is that the basic building blocks of DNA or RNA were initially present in the liquid prebiotic soup as monomers, i.e. individual molecular building blocks that combine (polymerise) to form a chain, where circumstances led to ligation of the molecules to form stable RNA or DNA strands. The monomers themselves could have originated from prebiotic material that is present in various types of geological material. The recent Hayabusa2 mission has even detected RNA nucleotides on the earth near asteroid (162173)Ryugu[36]. The probability of the molecules combining to bigger structures increases with their concentration in the surrounding medium, like a liquid, as a higher concentration means that the molecules meet more frequently. A promising environment, where this accumulation of molecules could have occurred is in rock crevices.

The Braun Lab team, located at Ludwig-Maximilians University in Munich, has designed a thermal trap that imitates natural rock crevices and allows for the examination of the conditions that favor the formation of larger genetic molecules. When this thermal trap is heated up on one side and simultaneously cooled on the other, a temperature gradient is established, causing the liquid within the chamber of the thermal trap to circulate. This circulation causes substances to gather differently along the three spatial axes. As a result, the distribution of substances changes in various parts of the chamber. As the enrichment depends on the specific properties of the substance circulating in the liquid, different substances can be examined to see how well they can be concentrated by convection, which provides information on the optimum conditions for the development of life in the rock crevice. A simple and easy model to imitate here would be a rock crevice with an inlet and outlet at the top or a closed chamber. Because the atmosphere of the prehistoric Earth was more transparent to UV radiation, the influence of radiation damage on the DNA that may have existed at that time is of particular interest.

For this work, the aspect of how the enrichment of DNA changes when it is damaged by UV light was investigated. DNA and RNA are sensitive to the absorption of UV light, which may lead to a change of their molecular structure. This change of structure has an influences on the chemical and physical properties of the substances as will be shown.

Here two thymine DNA nucleotides linked as a dimer were used, which can form stable so called CPD-damages and are well suited for the use in the thermal trap. Since UV light not only mutates DNA but also destroys it, the yield of damaged but intact CPD-DNA was increased by photosensitizing with acetone as a carrier. Damaged and undamaged dimers were then placed together in the thermal traps and the differences in thermophoretic behavior were analyzed using high performance liquid chromatography. It was shown that CPD-DNA tends to accumulate relatively more at the bottom of the chamber and while undamaged DNA is found more in the upper parts of the chamber.

2 Theoretical background

2.1 The molecular structure of DNA

The raw and basic genetic information of a living organism is stored within its nucleic acids in the form of RNA or DNA. These molecules are made up of just five elements: carbon, hydrogen, nitrogen, oxygen and phosphorus.
The information is encoded by stringing together different nucleobases - thymine (T), uracil (U), adenine (A), cytosine (C) and guanine (G) - as strands, of which thymine only occurs in DNA and uracil only in RNA [3].

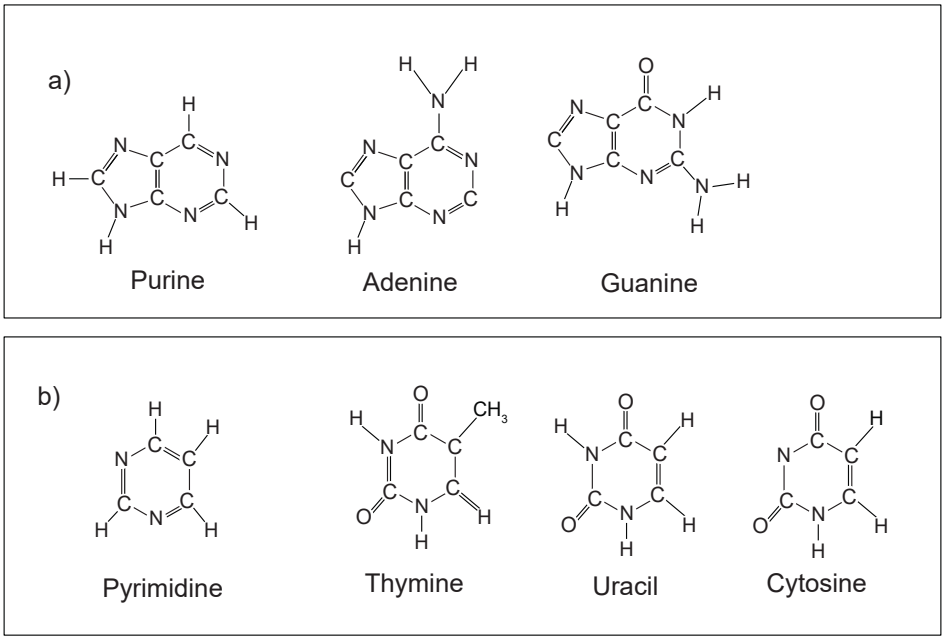

Fig. 1: Nucleobases based on purine (a) above and pyrimidine (b) below.

On these strands the nucleobases are each linked to the backbone of the nucleic acid, consisting of an alternating chain of sugar and phosphate molecules. In RNA the sugar is a ribose and in DNA a desoxyribose with the difference that the desoxyribose is missing an oxygen atom at the 2'-carbon atom. The nucleobases are coupled directly to the sugar molecule. A unit consisting of a nucleobase, a sugar and a phosphate molecule forms a nucleotide.

A single nucleotide is designated as a monomer, a molecule consisting of two connected nucleotides is called a dimer, few interconnected nucleotides are referred to as oligomer and many build a polymer. The start and end orientation of a single strand is determined from the 5‘ to the 3’ carbon atom of the sugar molecules in the backbone. [3]

Primary structure is a term that refers to the specific sequence of the linearly arranged bases that make up the DNA or RNA single strand. The strands can adhere to them-

selves or to other strands, forming three-dimensional secondary structures. The 1953 discovered double-helical form of DNA by Watson and Crick is an example of such a secondary structure: Two anti-symmetrical single strand DNA molecules couple together by bonding complementary base pairs with each other. Physiologically adenine bonds to thymine (or uracil in RNA) and guanine couples to cytosine. DNA typically exists as a double-stranded molecule, whereas RNA can occur in both single- and double-stranded forms. The resolution of two DNA strands into two single-strand DNA (ssDNA) is called melting with an increasing probability at higher temperature.[17]

Different molecular forces are at work within a DNA complex. In terms of binding energy, the covalent bonds of the sugar molecules form the strongest interactions, to which the phosphodiester bond with the phosphate molecules and the glycosidical bonds with the nucleobases belong. In double stranded nucleic acids two more forces are at work: hydrogen bonds are formed between the complementary base pairs of the connecting strands. On the individual loose strands themselves, the nucleobases would have the ability to rotate around the longitudinal axis of the strands. In double helical configuration neighboring bases are held together by Van-der-Waals forces, which is called base stacking. [3] The ability of nucleotides to rotate will become important later in Chapter 2.2.2 on UV damage.

2.2 Photolesions

2.2.1 Photosensitivity

Nucleic acids are sensitive to UV radiation, which can result in temporary or persisting damages to their structure. Those changes might influence evolutionary processes, which will later be examined with the help of the thermal traps.

The DNA/RNA absorption capacity of infrared radiation [14] is not further relevant for the creation of photoproducts, as the photon energy in this spectrum is with a maximum energy of

$$E = \frac{h \cdot c}{\lambda} = 1.77eV$$

at 700 nm wavelength not sufficient enough to induce relevant electronical excited states leading to photodamage. E.g. the first excited state for thymine is given as 4.55 eV. [25]. However infrared radiation plays an important role in investigating the structures of nucleic acids. [19]

Within the nucleotides, most of the UV radiation is absorbed within the nucleobases at wavelengths peaking between 250 nm and 270 nm, while the sugar-phosphate backbone shows a little increased absorbance at wavelengths below 220 nm. [26] A reduced absorption spectrum of monomers (without uracil) can be seen in Fig.3. The peaks with the highest absorbance lie in the UV-C spectrum (200-280 nm) and less absorbance can be observed in the UV-B spectrum (280-315 nm). [14]

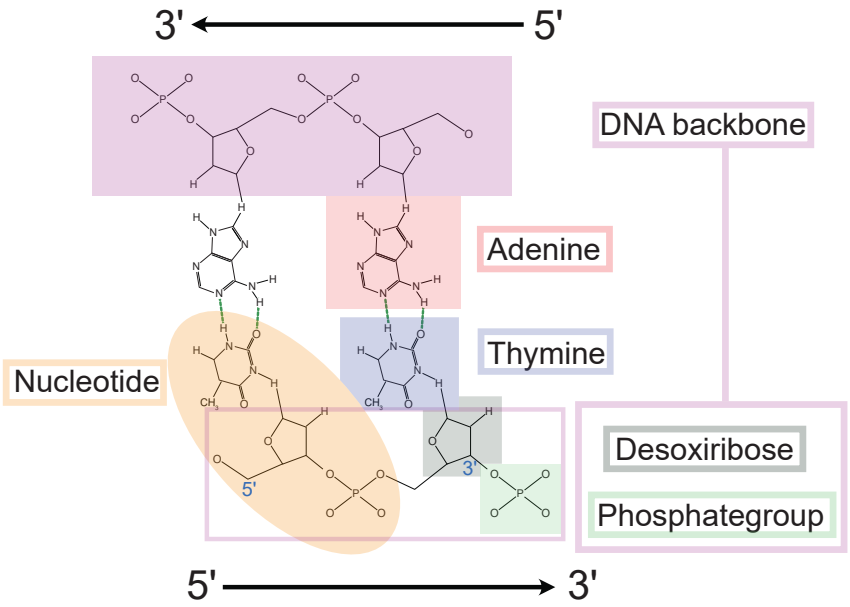

Fig. 2: Structure of DNA: schematic linking of two thymine (blue) nucleotides that are coupled to their complementary adenine (red) parts. The nucleobases are coupled to a backbone (purple) consisting of a chain of desoxiribose (grey) and a phosphate group (green). A single nucleotide (orange) consists of a nucleobase, a sugar and a phosphate group. The stands are held together by hydrogen bonding (green dashed lines). The strands have a 5' to 3' orientation, with the carbon atoms of the sugar molecule numbered starting from the base connection.

Due to the composition of organic material mostly from the few substances as described in Chapter 2.1, the valence electrons of the resulting molecular orbitals are located on binding (sigma, pi) orbitals, non-binding orbitals (n) or anti-binding (π^*, σ^*) orbitals. In chemical diagrams (e.g. Fig. 1), sigma bonds are shown with a single bar and pi bonds with a double bar. Non-bonding electrons are shown with a dot or dash that is only adjacent to a single element. Biophysical UV and visible spectroscopy primarily involves transitions between these orbitals. The excited electronical states always involve the π^* and σ^* orbitals, see Fig. 4. [20] A transition between to states with lower energy a and a higher energy b will in the following be denoted as ab.

In DNA most absorbed photons create electrons with $\pi\pi^*$ states, but most of these excited states rapidly decay through internal conversion back to ground state within a period of a few picoseconds. In internal conversion the excess energy of the electron is transferred into vibrational energy of the atom, that is exchanged with the environment leading to vibrational cooling. When falling back to lower levels of energy, pyrimidine bases (see. Chapter 2.1) show the ability to also populate $n\pi^*$ states with longer lifetime. [26]

Another process of decay happening is intersystem crossing from the singlet $^1\pi\pi^*$ state to

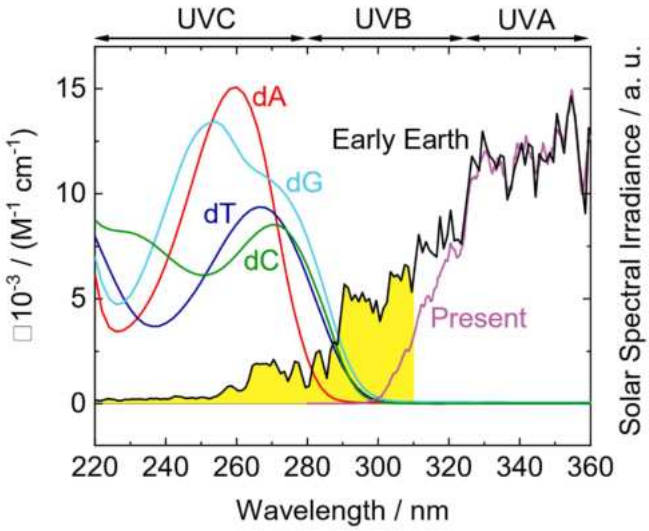

Fig. 3: Adapted from [14]: Absorption coefficients of deocynucleosides. The solar spectrum of early earth (black line) and present earth (violet) is overlaid.

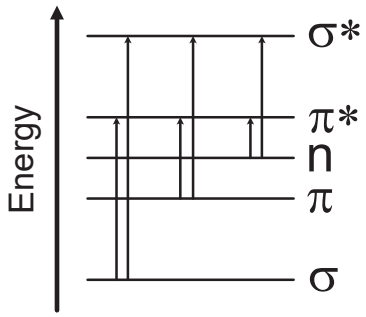

Fig. 4: Energy levels and transitions in organic compounds

a triplet ${}^3\pi\pi^*$ state, which is physically a lot more complicated. Usually these transitions are forbidden due to spin preservation. But a reduction of the energy gap between singlet and triplet state and an overlap of the vibrational states [11] enables this transition albeit with a small yield. [26] The quantum yield ϕ with the wavelength λ is defined as the ratio

$$\phi(\lambda) = \frac{\text{number of events}}{\text{number of absorbed photons}}.$$

where a event is a photochemical reaction leading to photodamaged DNA.[5]

Double stranded DNA and RNA show two special features. For one they have lower UV absorption coefficients in most spectral regions, as can be seen in Fig. 5 due to a better molecular stability. [26].
Additionally the excited electrons of the ${}^1\pi\pi^*$ state can delocalize over several bases or

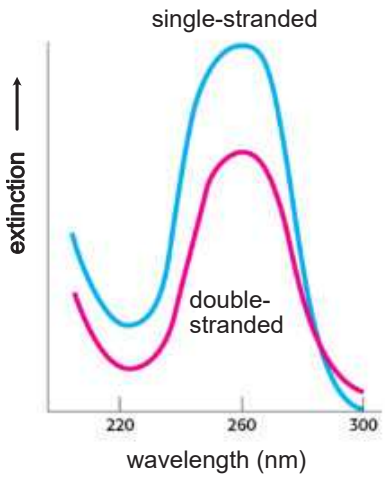

Fig. 5: From [3]: Single-stranded DNA shows mostly higher extinction coefficients than double-stranded DNA.

base pairs, forming an exciton. An exciton is a quasi-particle similar to a hydrogen atom, consisting of a negatively charged electron and a positively charged hole. Furthermore, the excited molecule can interact with a neighboring molecule in its ground state, forming an exiplex. This exiplex is a intermolecular excited state complex, which can open additional decay channels. Both the exciton and the exiplex (see Fig.6b, right side) states can contribute to molecular damage, as they can lead to energy transfer processes that create reactive photoproducts or chemical changes in the DNA structure. [26]
Because of the many pathways of elastic relaxation, the overall yield for the creation of photochemical products lies at around 1%. [26] In Chapter 2.2.3 photosensitization, a principle to further increase the yield for damaged DNA will be shown. The next chapter provides an overview of the various photolesions encountered in this experiment.

2.2.2 UV induced photolesions

Most DNA photolesion are made up by cyclobutane-pyrimidine dimers (CPD) (75%) and 6-4 photoproducts (25%) [29]. An exact and general overview of the frequency of the various types of photodamage in vitro or in vivo is difficult to determine because it depends on the measurement method and the circumstances of the irradiation. To better describe the frequencies it would be easier to determine the quantum yield of the photoproducts. [14] But as the other photodamages like spore products or oxidative 8-OxoG products only make up only a very small amount of photolesions and are of no further significance for the experiment, they will not be described further below.

The pyrimidine nucleobases (see Fig. 1) thymine and cytosine have the ability to form cyclobutane-pyrimidine-dimers. In this case, the bases involved bind covalently to each other at their C5 and C6 atoms and form a four membered cyclobutane ring. The cyclobutane ring can be composed in four different ways: The participating bases can be on

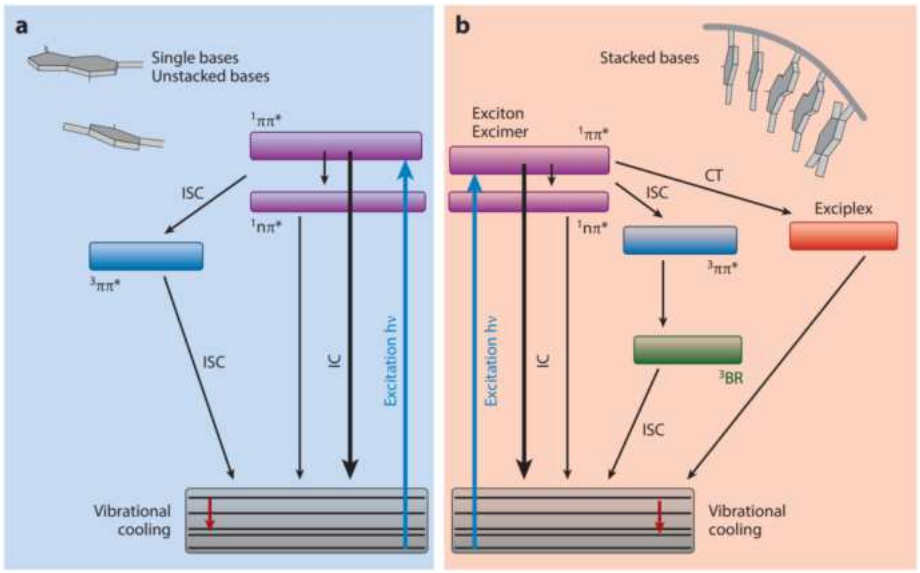

Fig. 6: Adapted from [26]: Non radiative transitions after UV excitation in isolated DNA bases (a) and single/double stranded DNA (b): internal conversion (IC), intersystem crossing (ISC) and charge transfer (CT). Most nucleic acid UV excitations decay through those processes followed by vibrational cooling. This reduces the yield for the creation of photoproducts like damaged DNA/RNA.

the same side (cis) or on opposing sides (trans) of the cyclobutane moiety. Additionally the C5 atoms, respectively the C6 atoms, can either couple with each other (syn) or C5 and C6 atoms can each bind crosswise (anti) with each other. When connected to a backbone the anti-configuration of the bases is restricted due to the lack of flexibility. [7] The cis-syn form is produced in large excess with respect to the trans-syn DNA dimers and the latter only occur in single stranded-DNA [21][33]. CPD lesions form at higher yields in single-stranded [7] or melted [32] DNA. The bonding of bases is easier at the flexible ends of adenine-thymine tracts, but not in their rigid center, as the rigidity prevents proper alignment of the molecules that have a rotational range of motion.
Among the possible pyrimidine base compositions — TT, TC, CT, and CC — TT dimers appear to yield the highest proportion of photolesions, with values ranging from 28% to 88% [7][14][24], depending on the method used and in particular, the radiation wavelength. As for the reasons, why thymine has a higher affinity for forming CPD lesions, thymine appears to be able to adopt more stable excited states that allow the appropriate paths of decay, which are necessary for the photochemical reactions that lead to CPD formation. Also the binding energy of TT-dimers is e.g. 3-fold higher compared to CC-dimers, which also have to surmount a 0.2 eV energy barrier even in excited state, unlike TT-dimers. [28] The CPD dimers are stable molecules. But ongoing irradiation with UV-C light can result in further changes like the reverse of the complex to the starting pyrimidine bases, C $\rightarrow$ T transitions in case of cytosine with deamination [21] or other structural damaging.

In terms of quantitative importance, the (6-4) pyrimidine photoproducts are the second most common type of lesions resulting from UV irradiation. They are formed at a rate

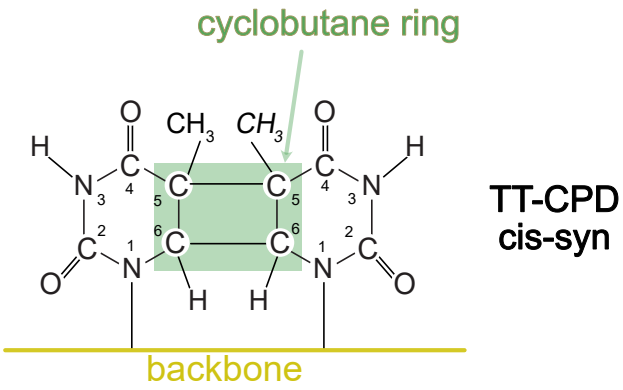

Fig. 7: Thymine-Thymine Cyclobutane Pyrimidine Dimer (TT-CPD): This dimer forms between two neighboring thymine bases on a single strand of DNA (backbone in yellow) and is in cis-syn configuration. In this formation, "cis" refers to the fact that both thymine bases are located on the same side of the DNA strand, while "syn" means that the bonds between the carbon atoms at positions 5 and 6 on both thymines are aligned parallel to each other. The cyclobutane ring is colored in green. Source: modified image from [8].

that is 20-30 % that of the cyclobutane pyrimidine dimers. [32] From a singlet excited state an unstable oxetane is formed and rearranged by establishing a bond between two carbon atom of the corresponding bases (see Fig. 8). The 6-4 damage is an insignificant byproduct in this experiment and of minor relevance.
As already explained in Chapter 2.2.1, DNA has the property to reduce its photo-optical excitations by elastic processes, making it a rather stable biological molecule. In order to produce larger amounts of TT-cyclobutane dimers to make them available for the experiment, a method called photosensitizing can be used, whereby desired decay pathways are preferred, leading to a higher quantum yield. This will be described in the next part.

2.2.3 Photosensitizing

Photosensitization can mean a number of different things, depending on the context and field (medicine, biochemistry,...) in which the term is used.
Here it is used to describe a process where a molecule (photosensitizer) absorbs light and then transfers its energy or an electron onto another molecule [34]. The special feature of the presence of a photosensitizer is that it enables additional reaction pathways or increases the probability of processes that would otherwise be unlikely. As mentioned in Chapter 2.2.2 pyrimidine bases are sensitive to UV light. But their excited states are short lived and tend to decay back to their original state through fast processes, making DNA a light stable molecule.
There are different activation mechanisms for photosensitization, but the most frequently described mechanism, which is also relevant for this experiment, is a triplet-triplet transition. Usually the ground state of organic molecules is the singlet state. By occupying longer-lived singlet states, compared to DNA, the photosensitizer molecule tends to undergo spin conversion and thus occupies a triplet state. Collision in turn stimulates the

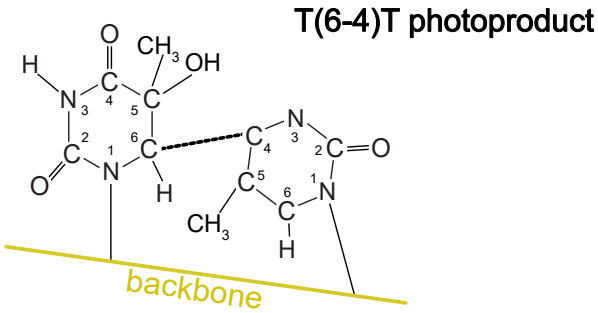

Fig. 8: The (6-4) photoproduct is the second most common photochemical product of DNA UV irradiation. The name is derived from the numbering of the bonding atoms in the pyrimidine ring and is created through various intermediate stages, starting with an excited singlet state of a participating pyrimidine base. This picture illustrates a thymine-thymine (6-4) dimer. Source: modified image from [8].

DNA into a triplet state, which is stable enough and provides enough time to form the cyclobutane ring. For this to happen the bases being able to rotate on the longitudinal axis of the backbone need to be in a proper neighborhood. After forming the CPD dimer the triplet state then decays to a singlet state again. An additional technical advantage of photosensitizing the samples in the laboratory is the lower needed excitation energy of the photons and therefore less destroyed DNA [12] [14]. From a medical point of view, of course, this has disadvantages, as DNA can mutate more easily when exposed to longer wavelength light like UV-A, as biological tissues contain natural substances that have a photosensitive effect. Although in contrast to the early Earth, today's ozone containing atmosphere [26] filters the UV-B and UV-C components out of the solar light (see Fig. 3), there are still non-negligible DNA damages done by UV-A through photosensitizing [34].
In this experiment, acetone is used as a photosensitizer providing a small range of photochemical products. Photosensitizing thymine-thymine dimers with acetone before illumination mostly generates cis-syn CPD-TT dimers and additionally a small number of 6-4 damages [18].

2.3 Thermophoresis

Particles concentrated in a liquid or gas that have a temperature gradient, show the phenomenon to move along or against the gradient. This phenomenon is called thermophoresis, thermodiffusion or Soret effect. The change of concentration is parameterized by the Soret coefficient S_T and described by the formula

$$c = c_0 \exp\left[-S_T(T - T_0)\right] \tag{1}$$

with the reference concentration c_0 at reference temperature T_0, the local temperature T and local concentration c and the Soret-coefficient S_T [22].

The Soret-coefficient is defined as

$$S_T = \frac{D_T}{D} \tag{2}$$

where D_T is the thermodiffusion coefficient described by the directed drift velocity of particles in a temperature gradient

$$\vec{v} = -D_T \nabla T \tag{3}$$

and the diffusion coefficient D which results from the Brownian motion i.e. the random tremor-like movement of particles in a gas or liquid, approximated for spherical particles by the Stokes-Einstein equation with viscosity η, hydrodynamic radius r, Boltzmann constant k_B and temperature T:

$$D = \frac{k_B T}{6\pi\eta r} \tag{4}$$

The hydrodynamic radius represents an increase of the radius of the particle resulting from the diffusive effect, which is caused by an accumulation of solution molecules at the particle radius, i.e. a layer of water wraps the particle which increases its physically effective volume.

The Soret coefficient increases linearly with the temperature and can assume positive and negative values. For positive values the particles move to colder regions and the opposite is true for negative values, see Eq. (1). [9] [35]
From a molecular perspective [35] [23] the determination of the Soret coefficient in aqueous solutions is a complicated matter. It depends mainly on the charge distribution of the molecules, which can be split up in a smaller non-ionic contributions, that can be neglected and several ionic contributions for charged molecules. Due to the dominantly negatively charged phosphodiester bonds of the backbone and the variable charged nucleobases (A,T,C,G), DNA molecules are negatively charged, with varying effect depending on the pH value of the surrounding solution described by the Henderson-Hasselbalch equation (see [35], p.7)).
The non-ionic contribution of the Soret coefficient depends on the molecular size and the viscosity of the solution. The more important ionic contributions are mostly the result of interactions between the Debye layer of the molecule and surrounding hydrodynamic forces. The Debye layer (see Fig. 9) is a term referring to the charged surface of the particle (negative for DNA), binding the free floating oppositely charged ions of the aqueous solution firmly to it as a charged layer. This hydratic double layer effectively increases the original particles volume while imitating a electrical capacitor with two planes charged positively and negatively. The (radial) electrical potential formed by the charged particle and its surrounding ionic layers is called Zeta potential, which assumes the value $1/e$ at the Debye length λ:

$$\lambda = \sqrt{\frac{\varepsilon k_B T}{\sum_{j=1}^{N} c_j q_j^2}} \tag{5}$$

with the permittivity ε of the solvent, the Boltzmann constant k_B, temperature T, the concentrations c_j of the ionic species and the corresponding charges q_j. Although this is a simplification, it provides a solid basis for calculations.

The Soret coefficient can be derived by the change of free energy W of the Debye layer in dependence of the temperature T [23]

$$S_T = \frac{1}{k_B T} \frac{dW}{dT} \tag{6}$$

For a detailed explanation see [35]. The differences of thermophoretic behavior of the damaged and undamaged thymine-thymine dimers used in this experiment result from the different Soret-coefficients. The Soret-coefficients are very difficult to evaluate theoretically, but could be experimentally retrieved, which is not part of this work.

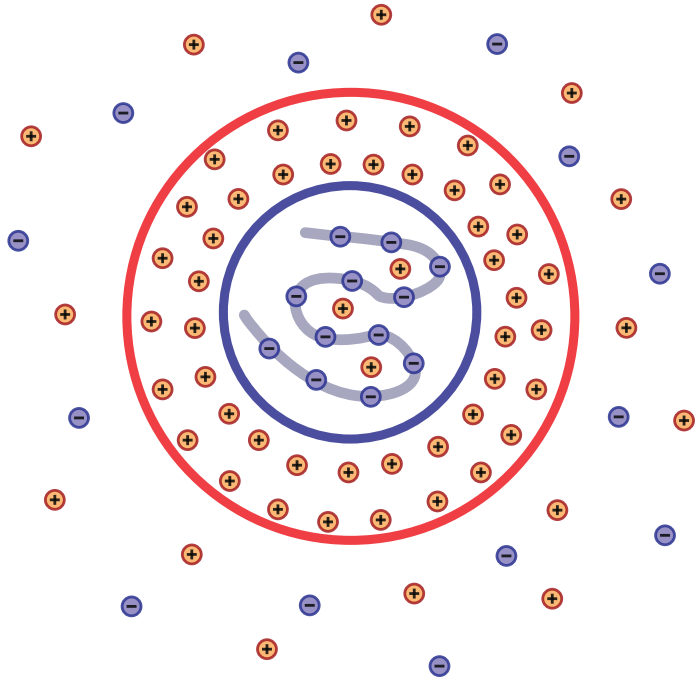

Fig. 9: In an electrolyte solution, where free floating cations and anions are present, charged polymers (such as DNA) attract oppositely charged ions, forming a surrounding layer. This results in two charged layers, one formed by the charged polymer and the other by the surrounding counter-ions, resembling an electrical capacitor. Source: modified image from [35].

2.4 Convection and circulation currents in chambers with a temperature gradient

While thermophoresis results in a steady-state concentration distribution of particles along a temperature gradient, convection refers to the transport of heat or mass caused by the bulk movement of fluid molecules driven by temperature-induced density differences [1]. If differences in temperature and concentration are aligned along horizontal layers, buoyancy effects appear through gravitational influence and an upward or downward flow appears. This flow can be a flow of heat, a flow of mass or both. Bejan et al. [2] have studied

this phenomenon in a fluid-saturated porous medium and found, that along a vertical wall with constant temperature T_0 the upward bulk velocity v of the liquid coming from a reservoir with temperature T_∞ yields

$$v = \frac{gK}{\eta} \left[\beta(T - T_\infty) + \beta_C(C - C\infty)\right] \tag{7}$$

Here g is the gravitational acceleration, K the permeability, η the viscosity, β and β_C are coefficients for thermal and concentration expansion and C_∞ is the concentration of the liquid from the porous reservoir. T and C vary spatially along their respective gradients. Thermophoresis and convection are movements, that happen linearly. [15] But interestingly from the combination of those two phenomena, when aligned perpendicular to each other, a circular fluid motion emerges, when the temperature gradient is established horizontally e.g. between two walls, see Fig. 10. Without limiting the generality and assuming a positive Soret coefficient, particles near the warmer wall tend to rise due to a lower density and move thermophoretically to the colder wall, where they sink again with their increased density and finally change over to the other side again, where the process starts from anew.

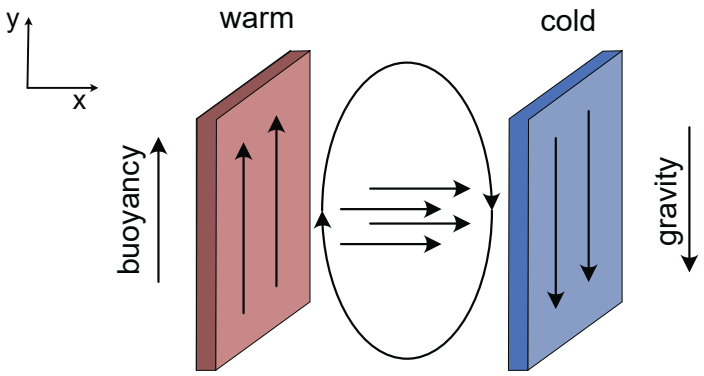

Fig. 10: Between two walls with different temperatures, a horizontal temperature gradient forms, driving thermophoresis between the walls. When these walls are aligned vertically, convection develops, resulting in upward or downward flow due to changes in density and buoyancy. The interaction of these horizontal and vertical movements, creates a circular flow of bulk motion between the walls [15].

Why is this circular motion of particular interest? Mast et al. [15] found that this circulatory flow in a closed chamber with a temperature gradient as described above, also called a thermal trap, favors the accumulation of substances, such as nucleic acid building blocks, dissolved in the solution in the upper or lower part of the chamber. The enrichment of these building blocks to high concentrations is a crucial requirement for simulating conditions that enable the emergence of life, as the probability of nucleotides binding to already existing polymers increases significantly with their concentration. The change in concentration is expressed by the formula

$$\frac{\partial c}{\partial t} = D\left(\frac{\partial^2 c}{\partial x^2} + \frac{\partial^2 c}{\partial y^2}\right) + S_T D \frac{dT}{dx}\frac{\partial c}{\partial x} + v(x)\frac{\partial c}{\partial y} \tag{8}$$

where the first term resembles diffusion (Brownian motion), the second thermodiffusion and the third convection with drift velocity v. Although the calculation of the concentrations at arbitrary times may become computationally intensive, an equilibrium of concentration settles after a long enough time. Also as can be seen in Eq. 8, the enrichment of substances strongly depends on the Soret-coefficient. So if the damaged (CPD) and undamaged TT-dimers have different coefficients, they should also accumulate differently within a thermal trap.

Following research showed, that the differential equation Eq. 8 could be further transformed, to obtain a expression with which the Soret coefficient S_T could be determined by comparison of computational simulations (COMSOL) and experimental results [16]:

$$c(y) = \exp\left(+\frac{\frac{q}{120}}{1+\frac{q^2}{10080}} S_T \Delta T \frac{y}{\alpha}\right), \quad q = \frac{\Delta T \beta g \rho \alpha^3}{6\eta D} \tag{9}$$

with expansion coefficient β, gravitational acceleration g, thickness of the chamber of the trap α, density/viscosity of water ρ/η and diffusion coefficient D as before.
From the positive exponent in Eq. 9 it follows for positive Soret coefficients that substances with higher coefficients S_T tend to accumulate more strongly in the upper compartments of the chamber, while those with lower coefficients are depleted in the upper regions and instead gather at the bottom.

3 Methods and instrments

3.1 UV-Laser setup

Fig. 11: Image of UV-Laser in laboratory: Ekspla NT200.

To expose the TT-dimers, an Ekspla NT200 diode pump laser was used, which is tunable in a wavelength range from 210 nm to 2600 nm, with a pulse length of 5 ns [1] [13]. The laser is cooled via external units and can be operated via a hand console.
The exposure time of the sample is controlled with a stopwatch and by opening and closing the aperture integrated to the laser. The beam is directed via mirrors onto a 50/50 beam splitter. The beam is split into a reference beam, which is directed onto a detector, and a sample beam, which is used to expose the sample (see Figure. 12).

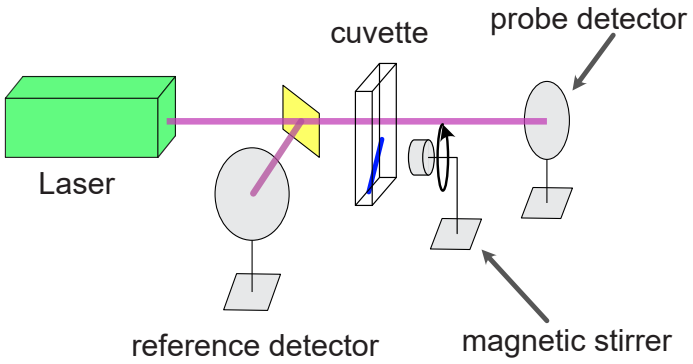

Fig. 12: Sketch of laser setup: The laser beam is split into a reference beam and a probe beam, to determine the dose absorbed by the probe. A magnetic stirrer moves a stirrfish inside the cuvette to expose the aqueous solution within the probe more evenly.

The sample itself is located in a cuboid cuvette (Hellma), which is placed in a holder with a custom made magnetic stirrer mounted on the back. For better mixing of the sample with more uniform irradiation of the DNA bases, a stirring fish was inserted into the cuvette. A further detector behind the sample records the sample beam, which is

[1] Since only the manuals of the successors of the NT200 are still available online, secondary sources had to be used for these specifications

attenuated by absorption in the probe. During the entire exposure, a program written in LabVIEW displays and saves data like the absorbed dose per base, evaluated from the detector signal, the probe parameters (quantity and concentration) and the laser settings (wavelength).

To obtain reliable values for the absorbance by the sample molecules, the measurement must first be calibrated with a cuvette filled with the same, but pure, aqueous solution as in the sample cuvette, only without target molecules.

The used cuvettes are optical instruments, that are transparent for UV light and have a maximum volume capacity of approximately 400 µl. Before usage they have to be cleaned with ethanol, 1% Hellmanex and acetone.

3.2 Gravitational thermal traps

Gravitational thermal traps (see Fig. 13) were developed by the Braun lab team LMU Munich. They can be used [16] to imitate the circulating movement of liquids in naturally occurring stone crevices. The space where the circulation is happening is defined by cutting out a chamber with a inlet and outlet for liquid from an fluorinated ethylene propylene (FEP) film. The chamber foil has a thickness of 170 µm and is cut out of a carrier foil in the laboratory by an industrial plotter device (CE6000-40 Plus, Graphtec, Germany). Two sapphire glasses coated with water-repellent surfactant (ProSurf MT-5) are enclosing and sealing the chamber. One of the glasses is thinner and has four laser-cut holes of 1 mm diameter through which the liquid can be supplied by tubes and syringes connected to suitable adapters such as UP P702-01 connectors and VBM 100.632 ferrules, for which suitable threads are milled into the rear housing. The glasses are held together by a metal steel frame for which the corresponding screws are tightened with torque spanners. A total of three graphite foils is placed between the components to ensure better heat transfer.

Before filling the chamber with the desired probe liquid containing the DNA bases, it has to be flushed with flourinated oil. The oil has a low viscosity and helps to check the chamber for leaks and pushes out gas residues. After the DNA liquid has been drawn up, the tubings are sealed with caps.

To build up a thermal gradient, the thermal trap is mounted with it's back on a cooling unit which is set to -25°C and complementary the heating element is screwed onto the front and set to 80°C. Like this the device is kept running for 18 hours which has been empirically proven to be a good time for the spatial concentrations to reach a state of equilibrium.

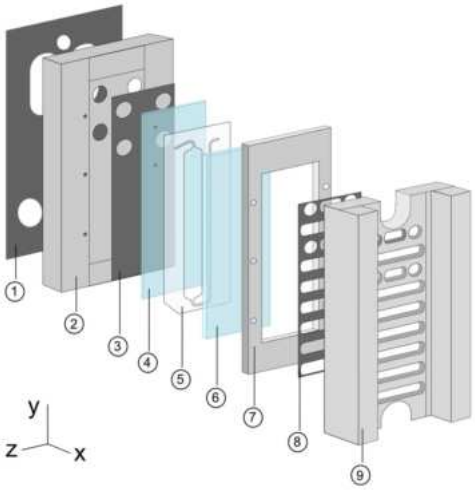

(a) Thermal trap: exploded view, from Matreux, Aikilla et al., Nature, 2024. [16]

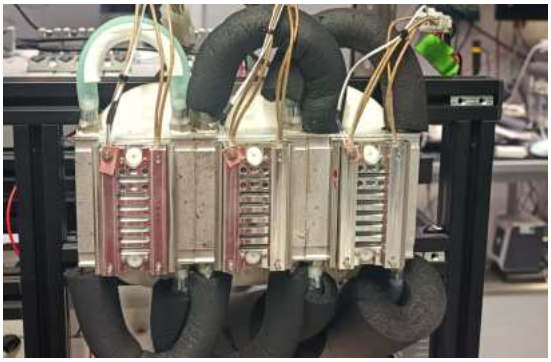

(b) Mounted on the cooling unit ready for operation

Fig. 13: Gravitational thermal trap: (a): The liquid-carrying chamber **(5)** is located between a thicker **(6)** and thinner **(4)** sapphire crystal. The thinner glass has laser-cut openings through which the chamber can be filled with tubes. The sapphires are screwed into a steel **(7)** and aluminum **(2)** housing from the front and back, with graphite foils **(3,8)** inserted between the glasses and the metals for better thermal conductivity. The electrical heating element **(9)** sits at the very front. (b) A graphite foil **(1)** is also placed between the back of the chamber, which is connected to the cooling element magnetically and with screws. The grid-shaped front could be used to take pictures of fluorescent particles, which is of no importance here. After switching on the heating (on the front, set to 80°C) and cooling (on the back, set to -25°C) elements, the trap runs for 18 hours until it is removed and shock-frozen.

3.3 Freeze extraction

A scheme of the liquid containing chamber where the circulation is build up, can be seen in Fig. 14. The circulation happens in the vertical back-front plane perpendicular to the image view, along the temperature gradient as sketched in Fig. 10. The substances dissolved in the liquid accumulate at different heights within the areas of the chamber depending on their Soret coefficients. The division of the chamber into five areas is arbitrarily. Once an equilibrium of concentration has been established, the trap is dismounted, the heater removed and the trap is quick-frozen at -80°C in a refrigerator for further analysis.

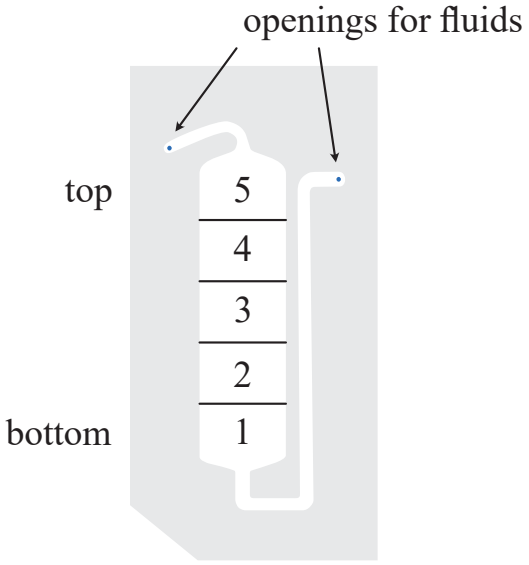

Fig. 14: Circulation Chamber: the heart of the thermal trap is the rock crevice imitating volume within the FEP foil. The chamber is for later analysis arbitrarily divided into five parts. Liquid can be added or exchanged through holes in the sapphire located in the upper part.

Next the metal frame is dismantled from the trap and the sapphires are separated from each other to get access to the now frozen core (see Fig. 15). A by the lab members self assembled and partly 3D-printed knife tool with razor blades helps to cut the chamber that is attached to one sapphire or distributed to both, into five pieces. With the help of three aluminum blocks at different temperatures, one frozen, one hot and one warm, unwanted melting is prevented and at the same time it is ensured, that only the desired areas of the chamber thaw, which are then pipetted into Eppendorf tubes.

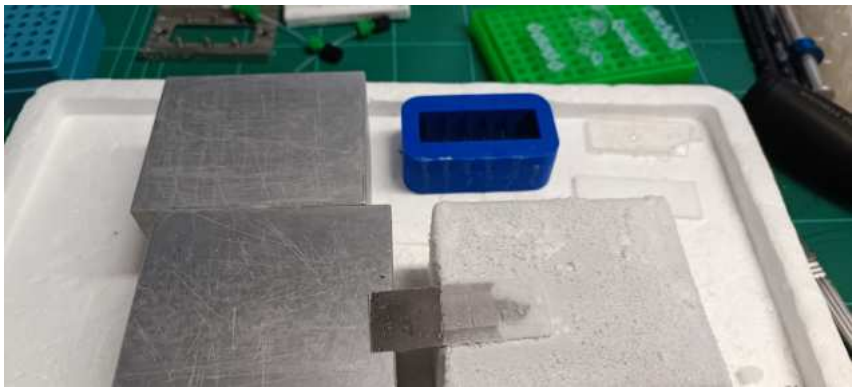

Fig. 15: Freeze extraction of the sample: To prevent the chamber from melting it is cooled with a low temperature aluminum block (on the bottom-right). It is then cut with the blue lab assembled tool (top-right) into five pieces. For a controlled melting of the desired sample, the sapphire is brought in contact with a moderately warmed aluminum block (bottom-left), that itself gets it's warmth from a hotter block (top-left). The sample is pippeted section by section into Eppendorf tubes/vials and analyzed with the chromatograph.

3.4 HPLC

Chromatography is a bio-technical computer-controlled technique used to separate substances dissolved in a liquid. The components of the sample to be analyzed flow through a column at different speeds, which enables beside the separation of the substances also their identification [4]. Alongside gel electrophoresis, it is one of the cornerstones of molecular biology with the advantage over electrophoresis that the substances may also be collected and their mass could additionally be determined by connected mass spectroscopy. In "High performance liquid chromatography" (HPLC) the term "high performance" implies the achievement of high purity and accuracy of the results of the procedure through a sophisticated improvement of the technology. [10]

The HPLC system is modular and consists of the following six main components, with the names of the Thermofisher instruments used in this experiment shown in square brackets: [31]

- autosampler for injecting the sample [VC-A12-A]
- eluents also called mobile phase with which the sample is pressed through the column
- pump that generates the pressure to push the liquid (mobile phase and sample) through the column [VC-P20-A]
- column thermostats with columns (the porous stationary phase) [VC-C10-A]
- Fluorescence detector [VC-D50-A] with diode array detector [VC-D11-A]
- chromatography data system [Chromeleon]

Fig. 16: Image of HPLC device. On The right is the column holder with the columns. Then from top to down: eluents in the bottles, detector, autosampler, pump.[31]

After entering the parameters in the Chromeleon analysis program, the autosampler removes the required quantity from the sample containers and injects them into the column. The pump adds the eluents (mobile phase) and together the mixture is driven through a porous column (stationary phase). A number of factors ensure the desired separation of substances (analytes) which are determined by the different affinities for the stationary and mobile phases. These are caused by the physio-chemical properties of the analytes, i.e. their size, polarity and volatility, by the polarity and charge of the stationary phase and by the interactions with the eluents. [31] In normal-phase chromatography a polar stationary phase is utilized and a non-polar mobile phase. Roughly speaking, this results in polar analytes eluting later than apolar analytes due to interaction with the stationary phase. In reverse-phase chromatography it is the other way around (see Table 1). [4]

Table 1: Polarization of stationary and mobile phase in chromatography

	stationary phase	mobile phase	elution of polar substances
normal phase chrom.	polar	non-polar	later
reverse phase chrom.	nonpolar	polar	earlier

With the correct chromatographic method, the substances leave the column one after the other and can therefore be detected separately. The ability to separate two analytes is called selectivity. The time a substance leaves the column is referred to as the retention time. Then an absorption spectrum of the sample is recorded in the detector, whereby peaks whose height, width and area can be calculated become visible as a signal. The whole data output of an HPLC analysis is called a chromatogram. [31]

There are two different methods for adding the eluents: the isocratic method, in which the composition of the eluents, of which there may be one or more, is kept constant. Or the gradient method, in which the composition of the eluents can be varied over time. The gradient method is more complex and difficult to calibrate, but gives better sensitivity. [31]

For this experimental setup the reverse-phase mode was used with the column mentioned above and two eluents as mobile phase:

- water (4l jar) with 5 µM ammoniumacetate (1542 µg) and 80 µl ammonium for a more alkaline pH
- methanol

When working with DNA or RNA, reverse-phase chromatography is commonly used due to its increased sensitivity. This is attributed to the hydrophilic properties of the sugar-phosphate backbone, which provides good water solubility, and the hydrophobic properties of the canonical bases, which cause them to interact with the non-polar stationary phase. [6]

Fig. 17 shows a screenshot of the flow-method used for all the HPLC measurements. The analysis starts with a water-ammoniumacetate mixture (yellow) for a more sensitive

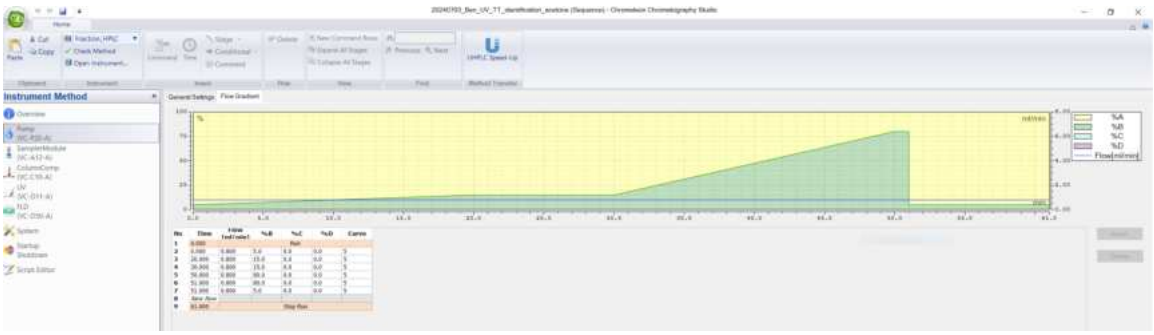

Fig. 17: HPLC flow method, proportions of eluents over the analysis time: mixture of water, ammoniumacetate and ammonia (yellow); increasing addition of methanol (green) towards the end of the program (change of gradient at 30 minutes for stronger elution.

elution of polar components. The increasing admixture of methanol ensures a stronger elution force for organic substances towards the end of the program. The overall flow rate remains constant at 0.8 ml\min

The detection of analytes in HPLC by recording an absorption spectrum is made more difficult by the fact that eluents such as methanol absorb radiation themselves. Each solvent is characterised by a cut-off in the absorption spectrum (see Fig. 18), above or below which 90 % of the input radiation is absorbed. Methanol begins to absorb significantly at 250 nm and has it's cutoff at 205 nm [27] just like ammoniumacetate.

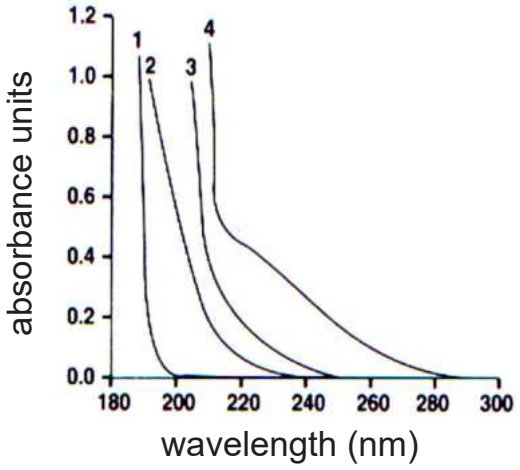

Fig. 18: Cutoffs for different solvents used in HPLC: 1: acetonitrile, 2: hexane, **3: methanol**, 4: tetrahydrofuran. (From [27]

The HPLC device is a sensitive and very prone to errors. As the one used at the start of the experiment did not provide any meaningful measurements, several things had to be checked and corrected with the help of the supervisor. Initially, there was a lot of noise in the signal, which could not be corrected by cleaning the column as recommended by the manufacturer. The insertion of a new column, the cleaning of the detector and several other things provided a good result. The differences can be seen in the Appendix (irradiation series of water and acetone at long times).

3.5 Photosensitizing

As explained in Chapter 2.2.3, higher concentrations of damaged TT-CPD DNA can be obtained by photosensitizing. For this, the used cuvettes were first cleaned with Hellmanex (1%), acetone and ethanol and then filled with an 1 mM TT-DNA aqueous solution and acetone in a ratio of 4:1 (e.g. 280 µl TT solution and 70 µl acetone, for a 350 µl starting volume). After UV-irradiation with a wavelength of 313 nm, the samples were pipetted into larger Eppendorf tubes and freeze-dried (Genevac EZ-2, see Fig.19a) until the liquid had completely evaporated and the dried DNA remains on the bottom of the vessel. The solution is then diluted again with the same amount of water as in the beginning (280 µl nucleobase-free water), vortexed and centrifuged. As an end result a small drop of liquid is obtained (see Fig. 19b), that can be further diluted or pulled directly into the thermal trap.

(a) Freeze-evaporator Genevac EZ-2

(b) Eppendorf tube with drop of final solution

Fig. 19: Freeze drying of photosensitized sample

3.6 Chromeleon data extraction

The Chromeleon software program enables both the control of the HPLC device for automated analysis of the samples and the direct processing of the data obtained. While passing the stationary phase, the substances within probes to be analyzed get separated and are registered by the software as peaks, where the data of retention time, the peak height and calculation of the area under the curve can be outputted. Fig. 20 shows a screenshot of the program used to analyze the samples collected from the thermal traps of the final study. Measurement data can be extracted to a text file, outputting the signal at a specific wavelength over time, or the entire absorption spectrum of the detection at a specific time.

Fig. 20: Chromeleon: screenshot of data analysis. Yellow markers: (1): area computation of peak; (2): specification of time for data output; (3): contour plot of detection signal; (4): absorption spectrum at specific time; (5): numerical output of predefined data points

4 Results

Some preliminary measurements had to be made prior to the actual experiment to investigate the separation of damaged and undamaged DNA in the thermal traps. This includes finding the optimum exposure time for UV irradiation to generate photoproducts, determining the detection wavelength for analysis and specifying photosensitization. The results for the latter parameters are only determined quantitatively, i.e. without repeating the tests and only with rough accuracy, as this would otherwise go beyond the scope of this work.

4.1 Time series of UV radiation without photosensitizing

Fig. 21 shows an overlap time series of the formation and degradation of photoproducts through UV irradiation at 266 nm without photosensitization. After each exposure step, 20 µl of the 500 µM TT solution was pipetted out of the cuvette originally filled with 350 µl, so that the total amount of DNA present decreases steadily at the same irradiation power. The individual plots for each exposure time and the rest of the data for this chapter can be found in the Appendix.

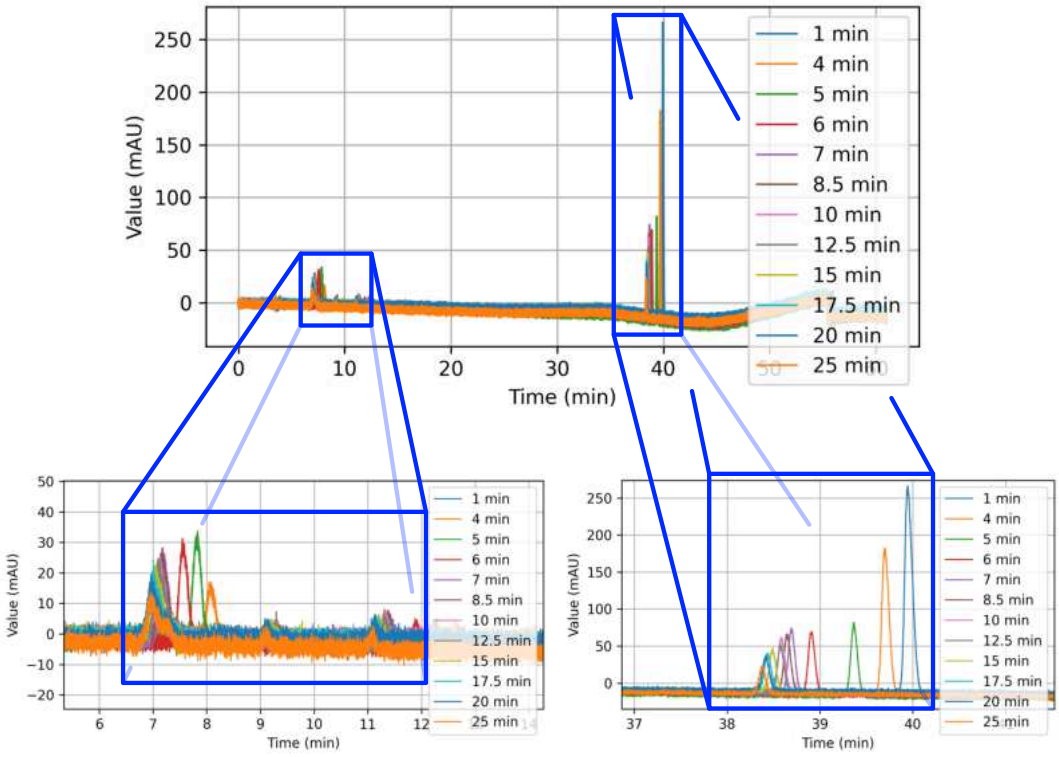

Fig. 21: Time series of UV exposure at 266 nm of TT in water with a concentration of 500 µM. Above: whole chromatogram. Below: Section of the areas where the peaks with CPD damage (left) and the peaks with undamaged DNA are located (right).

Based on the findings from Chapter 2.2.2 (photolesion) the peaks were identified as undamaged DNA, CPD-damages and 6-4-damages. Due to high noise, no signal could be

retrieved for CPD and other damages at 1 minute exposure time. The amount of analyte, which is equivalent to the surface under the peak, decreases continuously and non linearly for undamaged DNA. The amount of photoproducts first increases and then begins to decrease after 8.5 to 15 minutes of exposure with some fluctuation. Simultaneous degradation and new formation of photoproducts appears to take place. Beside a parallel shift of all three peaks at the beginning, the retention times are rather constant (see Fig. 22b and App. A.1.1).

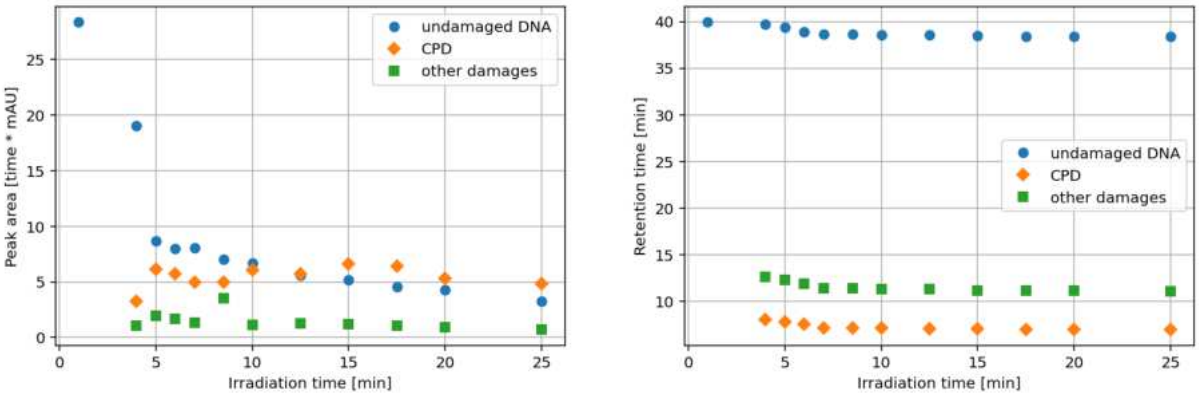

(a) Kinetics **(b)** Retention times

Fig. 22: Left: Kinetics of the formation and degradation of DNA photoproducts under irradiation. Over time, the amount of undamaged DNA (blue) decreases, while the amount of photoproducts - CPD (orange) and 6-4 (green) increases. At the end of irradiation, there is a similar amount of CPD and undamaged DNA. **Right**: Retention times of peaks at different exposure times. After an initial shift, the retention times are relatively constant.

4.2 Absorption spectra at peak maxima in the chromatogram

The absorption spectra of the photosensitization studies with acetone at 8 minutes exposure time at 313 nm are shown in Fig. 23. While the peak corresponding to undamaged DNA has two local maxima in the UV absorption spectrum, the other two peaks have only one. The negative values for the 6-4 damages are an artifact that could result from less absorbance of the sample than the mobile phase. [30]. The excitability of the damaged DNA decreases greatly (more for 6-4 damage than for CPD) and the wavelength of the excitation maximum shifts to lower wavelengths compared to the original DNA. But the excitability of the undamaged DNA is still higher throughout the whole spectrum.

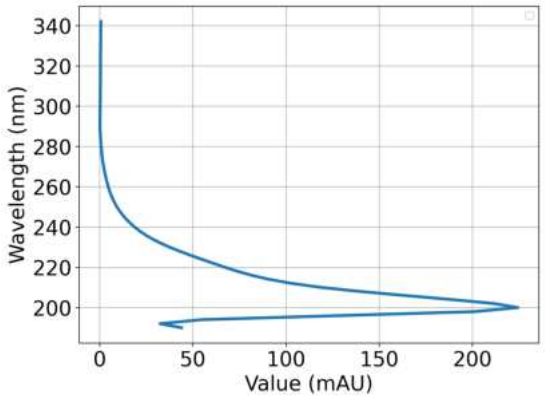

(a) CPD damage

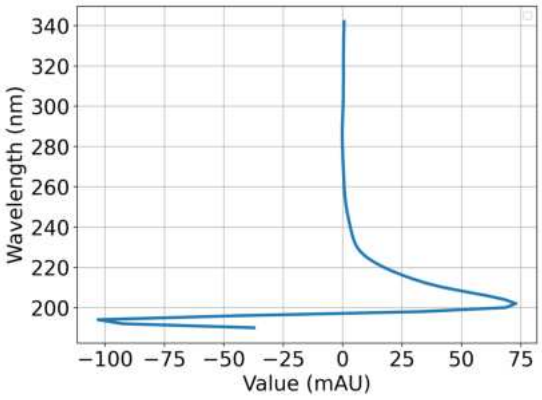

(b) T(6)-(4)T damage

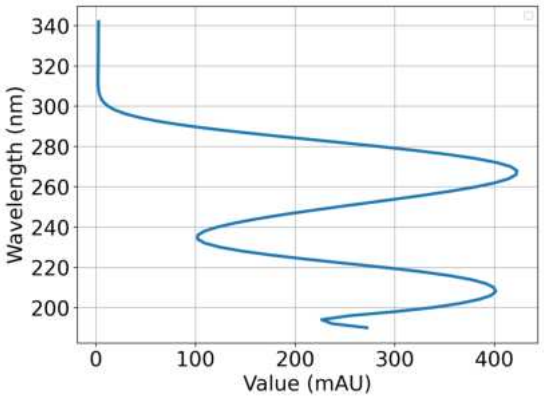

(c) undamaged DNA

Fig. 23: Absorption spectra of analytes at three different times centered at the detected peaks, arranged in ascending order of retention time. Plotted in arbitrary units (AU) versus wavelength. From acetone photosensitization study at 8 minutes UV irradiation with 313 nm wavelength.

Based on the absorption spectrum, the best detection wavelength for CPD damage appears to be around 200 nm. However, adjusting detection wavelengths below 220 nm first shows an initial tilt of the signal baseline to the right (see Fig. 24), followed by a tilt to the left for even shorter wavelengths. Partial overlap of the absorption spectra of the analytes and eluents makes it necessary to detect at wavelengths higher than the optimal 200 nm.

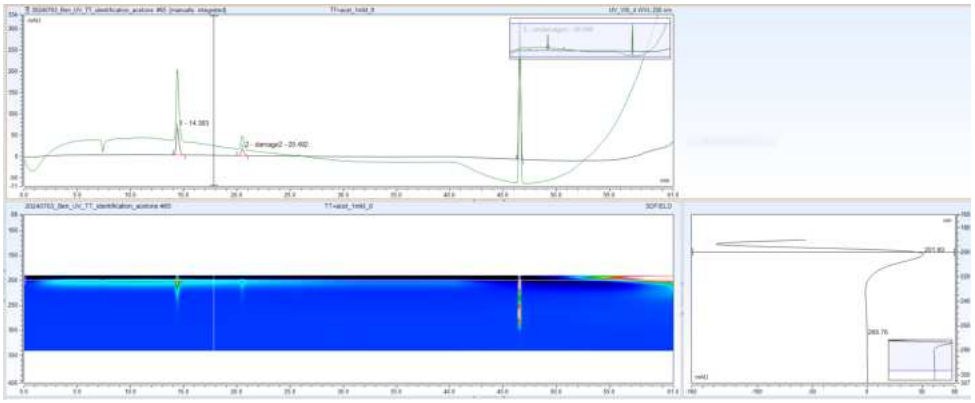

Fig. 24: Screnshot of Chromeleon with baseline slope at low detection wavelengths ($\sim$ 200 nm, green graph), which would be favorable for detection of CPD and undamaged DNA and signal at 220 nm (black graph) with flat signal. The absorption maxima of the eluents and analytes overlap at lower wavelengths.

4.3 Timeseries of UV radiation with photosensitizing

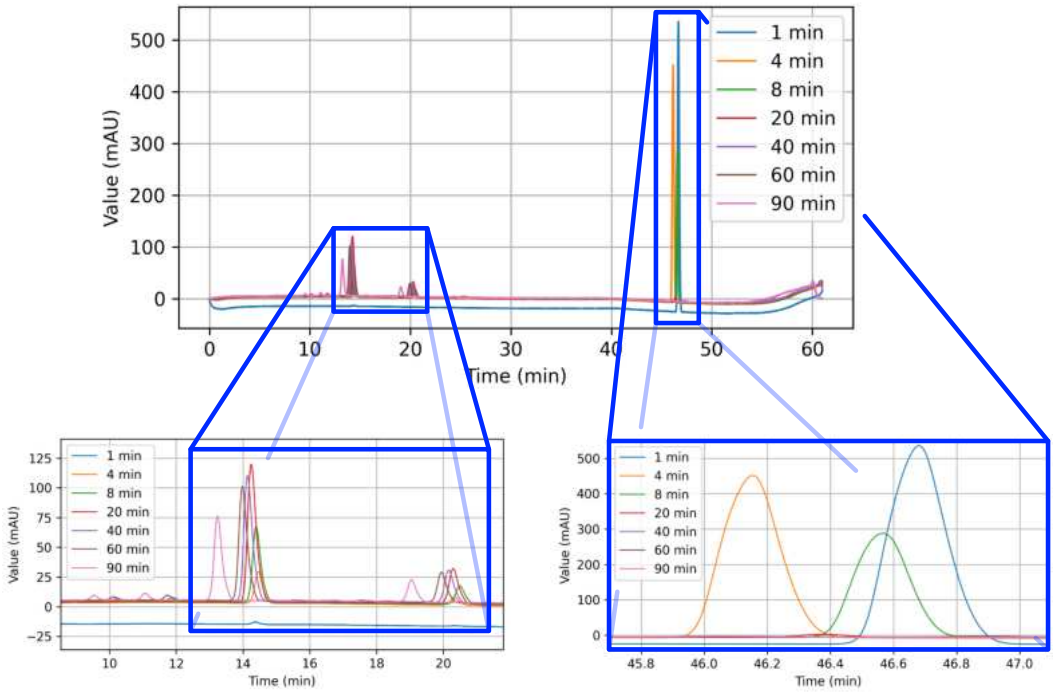

5

Fig. 25: Time series of UV exposure at 313 nm of TT photosensitized with acetone. Above: whole chromatogram. Below: Section of the areas where the peaks with CPD damage (left) and the peaks with undamaged DNA are located (right).

The original TT dimers are almost completely degraded after 20 minutes of exposure, coinciding with a simultaneous maximum in the formation of CPD and 6-4 photoproducts. Just like before, a lot more CPDs than 6-4 oligomeres are build in the process. After 40 minutes of exposure, the undamaged DNA has been fully converted, while the concentration of photoproducts begins to decrease steadily.

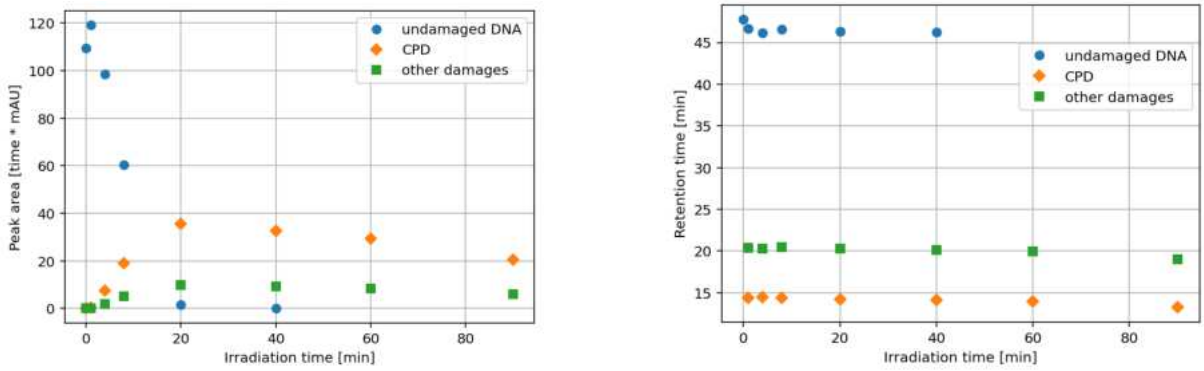

Fig. 26: Left: Kinetics of the formation and degradation of DNA photoproducts under irradiation. The amount of undamaged DNA (blue) decreases constantly and is no longer detectable after 40 minutes. The amount of CPD (orange) and 6-4 damage (green) reaches its maximum after 20 minutes and then slowly decreases. **Right:** Retention times of peaks at different exposure times are relatively constant and decrease slightly towards the end of irradiation.

4.4 Results of thermal trapping

Two sets of three traps were prepared for the experiment. From the first set, a lot of sample volume (20 minute irradiated DNA, 313 nm) was lost due to syringe leakage, so there was only enough sample left for filling one trap. Therefore, to allow more room for errors when filling the traps, the stock for the second set was doubled by dilution (originally 1 mM TT-DNA) with nuclease-free water after the entire photosensitization process.

During freeze extraction the 4th section of the 2nd trap mixed with surrounding condensation water and was mainly lost. They are therefore not included in the calculations. The profiles of distribution for each single trap can be seen in App. A.2.4 and the corresponding data is stored in App. A.2.3.

The ratio of the amount of substance found in each section to the total amount of the specific substance (CPD and undamaged DNA) was evaluated. The mean values of the ratios were determined (four measurement values for each section, except three for the fourth section) as well as the standard deviation for the error bars. Fig. 27 shows the results of the distributions in the thermal chamber and Table 2 the corresponding data.

Table 2: Distribution of the amount of substance within the chamber sections in relation to the total amount in (%).

	I	II	III	IV	V
undamaged DNA	85.47 ± 3.85	9.34 ± 1.86	2.93 ± 1.03	1.57 ± 0.38	1.07 ± 0.37
CPD	91.46 ± 2.65	6.58 ± 2.10	1.22 ± 0.55	0.53 ± 0.06	0.35 ± 0.12

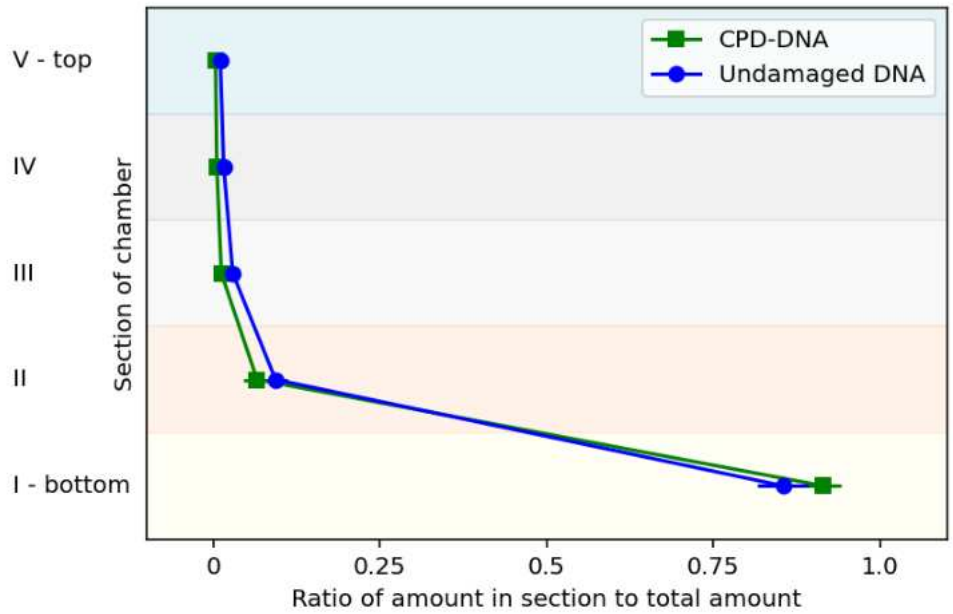

Fig. 27: Enrichment of substances (green: CPD-dimers, blue: undamaged DNA) in the five different sections of the circulation chamber of the thermal trap. The values are given as ratio of the amount of the specific substance found in the section, to the total amount of substance found in the whole chamber.

The enrichments can be compared by forming ratios of the relative amounts of each substance. This is shown in the heat map in Fig. 28. There is 7% more damaged DNA in the bottom section, while undamaged DNA accumulates more in the remaining chamber, with CPD having a distribution of only 33% versus undamaged DNA in the top section.

Even if the assessment of the 6-4 damage is not relevant for this work, an additional heat map was added for the sake of completeness with Fig. 29, which also takes this damage into account. Irradiation produces sufficient quantities of 6-4 photoproducts to qualitatively represent the pattern of inverse accumulation of the substances within the chambers: If one substance accumulates more at the bottom than another, it accumulates less at the top.

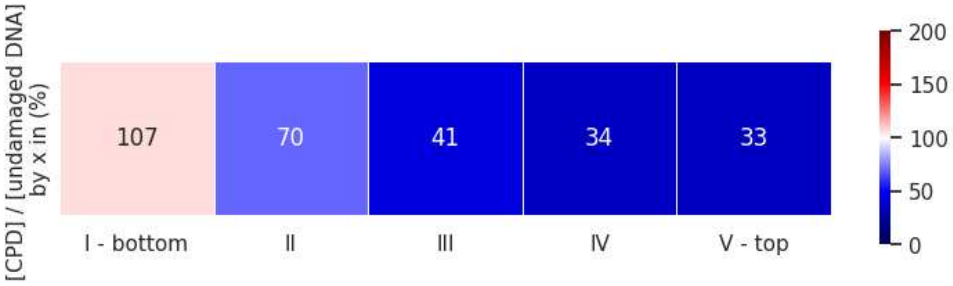

Fig. 28: Enrichment of UV-irradiated DNA dimers (CPD) over undamaged dimers, expressed as the ratio of the mean amount of the two substances found in each section. Due to the large difference in the distribution of the absolute mass fractions in the chamber and the fact that the majority of the masses of both substances are located at the bottom, small mass changes at the bottom mean large changes in the conditions for the rest of the chamber. This results in this large deviation of the percentage values in the vertical direction.

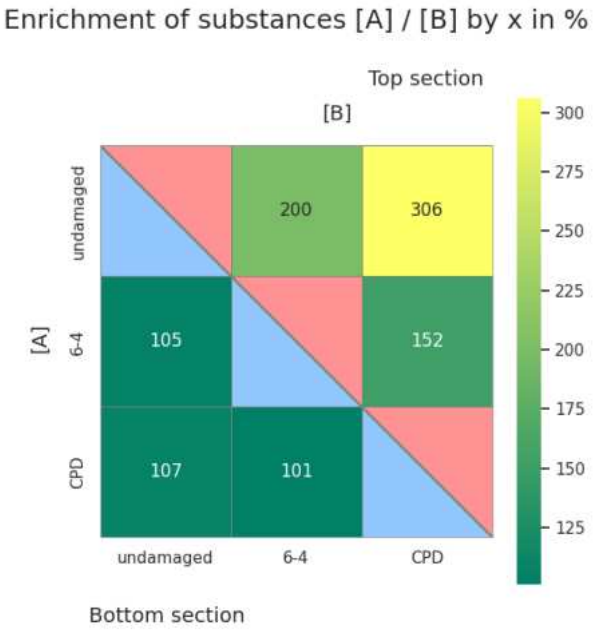

Fig. 29: Comparison of enrichment of all three different substances in the bottom section of the chamber (lower left triangle) and the topmost section (upper right triangle). The intermediate areas (sections II to IV) are omitted. The values are given as ratio [A] / [B] of the ratios of the substances. A qualitative symmetry is recognizable, in the sense that a sequence for the accumulation of the substances in the corresponding areas (top/bottom) is formed and this sequence is inverted in the two areas.

5 Discussion

Comparing the results of the irradiation with photosensitization (acetone) and without (water), various things become apparent. Firstly, the stronger noise in the water irradiation increases an inaccuracy not in the determination of the retention times, but in the peak area. The retention times decrease continuously in both series with few exceptions and converge to stable values (see App. A.2), indicating temperature fluctuations or similar disturbances in the HPLC device.

It becomes evident that photoproducts are much better preserved through photosensitization in contrast to irradiation without acetone. The absorbance (see Fig. 23) is significantly lower for all three dimer types at 313 nm (acetone) compared to irradiation at 266 nm (water), which apparently leads to less destruction of both converted and original DNA. The low absorbance of CPD and 6-4 dimers at 266 nm, seems to be enough for them to be broken down or converted back to their original state.

The process of photosensitization in itself was a success. However, the experimental setup does not yet allow any statement to be made about the actual concentration of the substances, as only a non-normalized detection signal, that scales differently for CPD and undamaged DNA, was used. So no information about the actual mass fractions is provided. This would require mass spectroscopy, for which collectable quantities of irradiated substance would have to be produced with a stable enough retention time. But although the work was not done with the same amount of mass fractions and the analytes may have interacted during circulation due to the rather high concentrations within the trap, as is known from previous experience [16], the height distributions of the analytes show an exponentially decreasing behavior (see App. A.2.4) as would be expected from Eq. 9. If it turns out that lower concentrations in the thermal traps would give better results for the Soret determination, one could try to reduce the detection signal to 200 nm by trying other eluents with a better cutoff, such as acetonitrile or hexane, or by supplementing the ammonium acetate.

The final data shows a slightly stronger accumulation of damaged (CPD) versus undamaged DNA in the lowest part of the chamber (7.0%), while undamaged DNA accumulates significantly more in the upper regions of the chamber, up to a maximum of 306.4% against CPD. In the case of a stone fissure, which would have its fluid inflow and outflow at the top like described in Chapter 1 (Introduction), this would mean that damaged TT dimers would be more likely to settle at the bottom reaching higher concentrations, while undamaged dimers would be more likely to be washed away, which would be disadvantageous for the ligation of those undamaged TT-dimers at the bottom of the downwardly closed gap. For the emergence of life, this would maybe be beneficial if CPD-TT has a comparable equal or greater probability of polymerization and if the healing of the photodamage can effectively be reversed by further UV irradiation or in the environment existing catalytic enzymes.

But the idea of a single rock crevice with an upper inflow and drain is too simple to

make any assumptions about whether the tendency to circulate in a thermal chamber is beneficial to the emergence of life, since natural environments are more complex than that [16]. Healthy dimers e.g. could be washed away and accumulate further downstream in a complicated network of fissures

Thermophoresis itself is also a process that is not fully understood, and understanding the change in Soret coefficient due to changes in molecular structure may provide new insights into the behavior of circulating fluids. The decrease in retention time for irradiated DNA suggests that damaged DNA is more polar than undamaged DNA, as polar substances are eluted earlier in reversed-phase mode HPLC (see Table 1). Dimerization appears to weaken the hydrophobic effect of the DNA bases and promote the formation of hydrogen bonds around the backbone (see Chapter 2.3). The next step would be to use T-oligomers larger than dimers or cytosine and uracil, which are also capable of forming cyclobutane rings. These bases could be tested directly for their suitability for the experimental setup and, if necessary, adapted with little effort.

6 Conclusion

The thermophoretic properties of thymine dimers and their accumulation in a gravitational thermal trap are altered by degradation to CPDs by UV irradiation. With 7%, damaged DNA tends to accumulate slightly more at the bottom of the gravitational thermal trap, than undamaged DNA, whereas undamaged DNA accumulates at the topmost part of the chamber by a far larger factor of three. In a single stone fissure with an upper inflow and outflow, undamaged DNA would be more likely to be washed away, which would lead to a lower accumulation of material for polymerization at the bottom of the chamber. Dimerization appears to inhibit the effect of the hydrophobic properties of the nucleobases on the molecule and therefore a larger hydration shell is build around the molecule due to the higher polarity, resulting in a smaller Soret coefficient with less participation in the convection currents.

The experimental setup is not yet fully developed for various reasons. Photosensitization with acetone has already generated sufficient CPD material to detect mass fractions in the upper chamber, but only statements about relative mass fractions could be made, as the detection signals have not yet been normalized, for which mass spectroscopic methods would be required. Therefore, the same amounts were not used for the enrichment of damaged and undamaged DNA, which could lead to inaccuracies in the comparison. Nevertheless, the exponential distribution of the concentrations over different heights of the chamber could be demonstrated experimentally.

CPD damage is relevant to the evolution of life because although DNA has many different elastic pathways of decay and is therefore relatively stable against UV radiation, photodamage is still happening frequently, and even more so on ancient Earth with a more UV transparent atmosphere. Cyclobutane pyrimidine dimerization of thymine and cytosine are the most common photodamages. However, these damages are reversible, on the one hand by the action of photolyases, like it is happening many times a second in our skin when exposed to sunlight, but also even without photolyases by further UV irradiation.

A Appendix

A.1 Chromatograms of UV irradiance time series

A.1.1 TT in aquaeous solution without photosensitizing

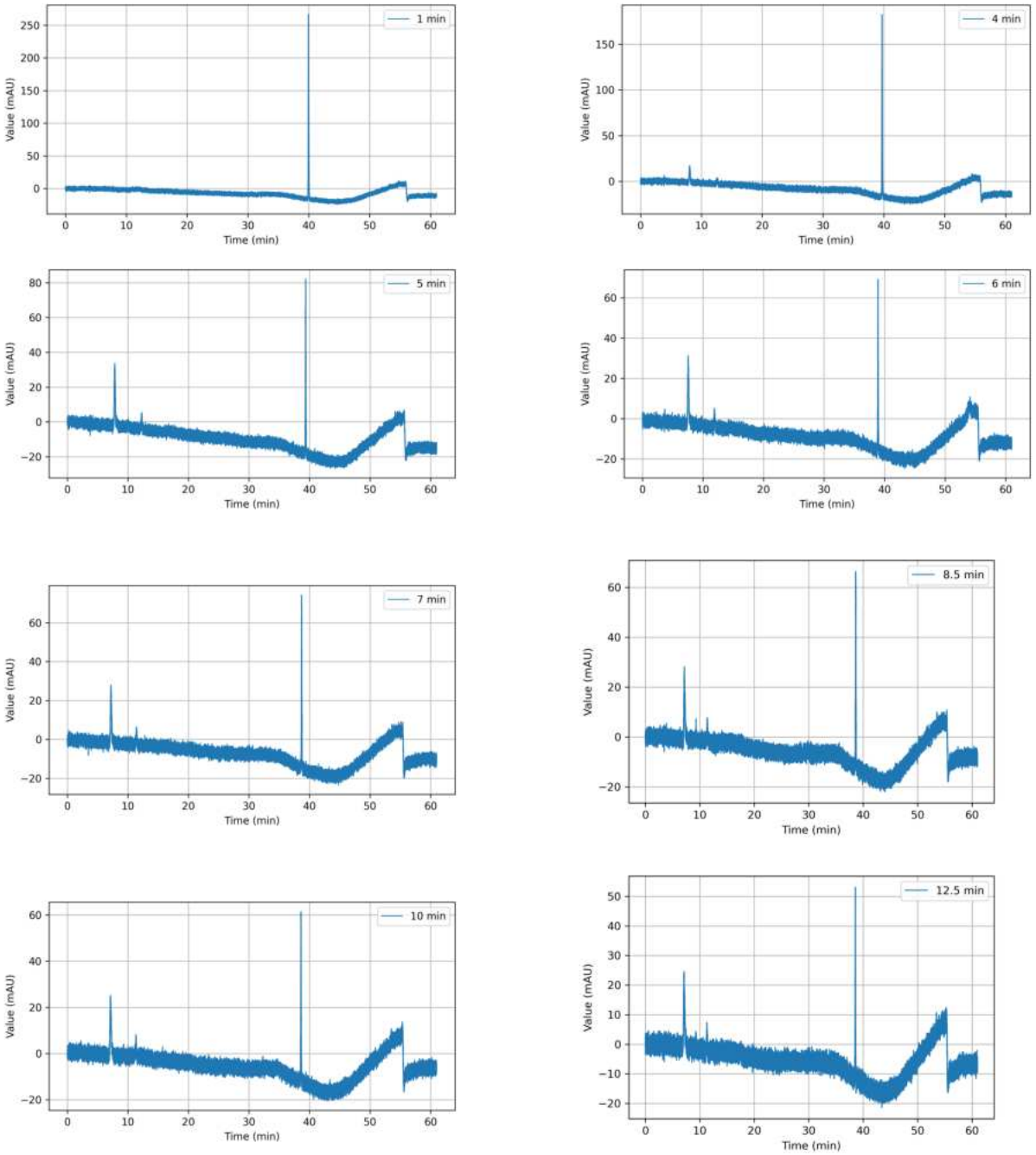

Fig. 30: Part 1: time series of UV irradiation at 266 nm without photosensitisation measured by HPLC at 220 nm. TT concentration in the aqueous solution: 500 µM. Mixing ratio water:acetone = 4:1. Starting volume 390 µl, 30 µl liquid was removed after each exposure step.

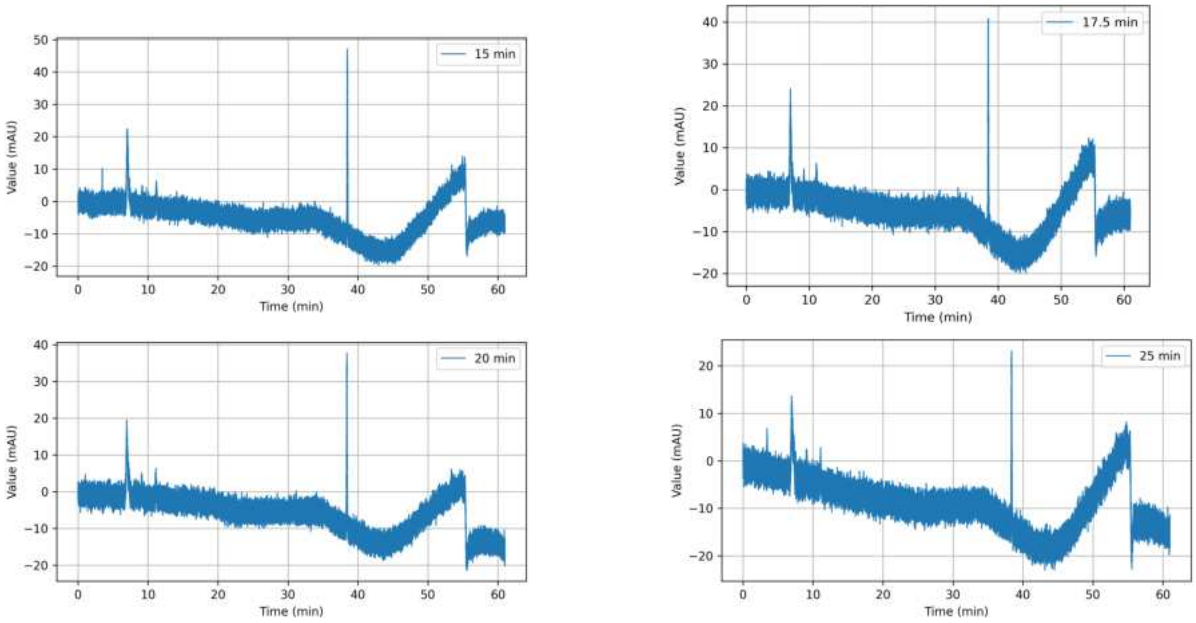

Fig. 31: Part 2

A.1.2 Photosensitizing with acetone

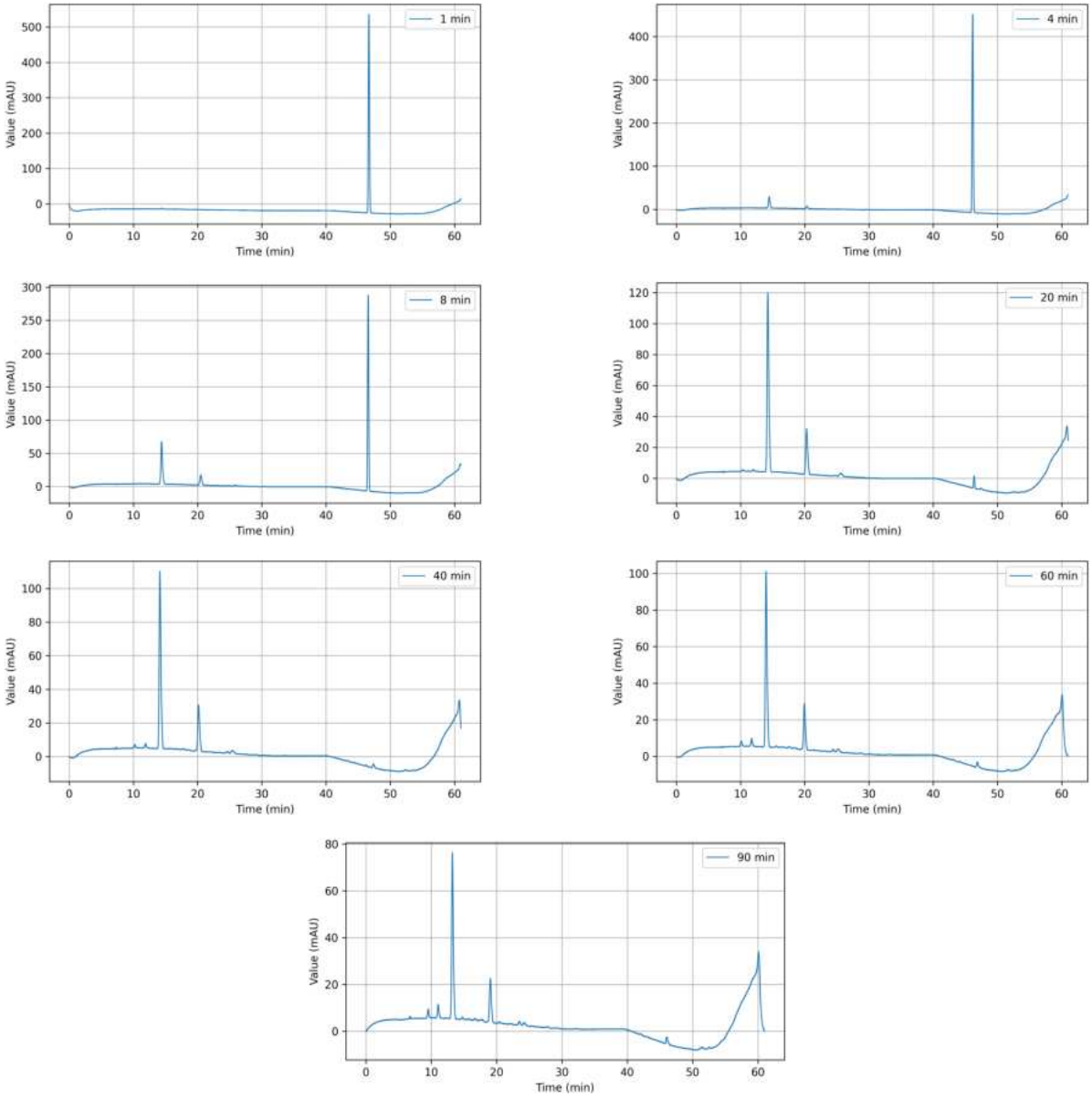

Fig. 32: Time series of UV irradiation at 313 nm with acetone photosensitisation measured by HPLC at 220 nm. TT concentration in the aqueous solution: 1 mM. Mixing ratio water:acetone = 4:1. Starting volume 390 µl, 30 µl liquid was removed after each exposure step.

A.1.3 Chromatograms of different sections of thermal traps after thermocirculation in ascending order

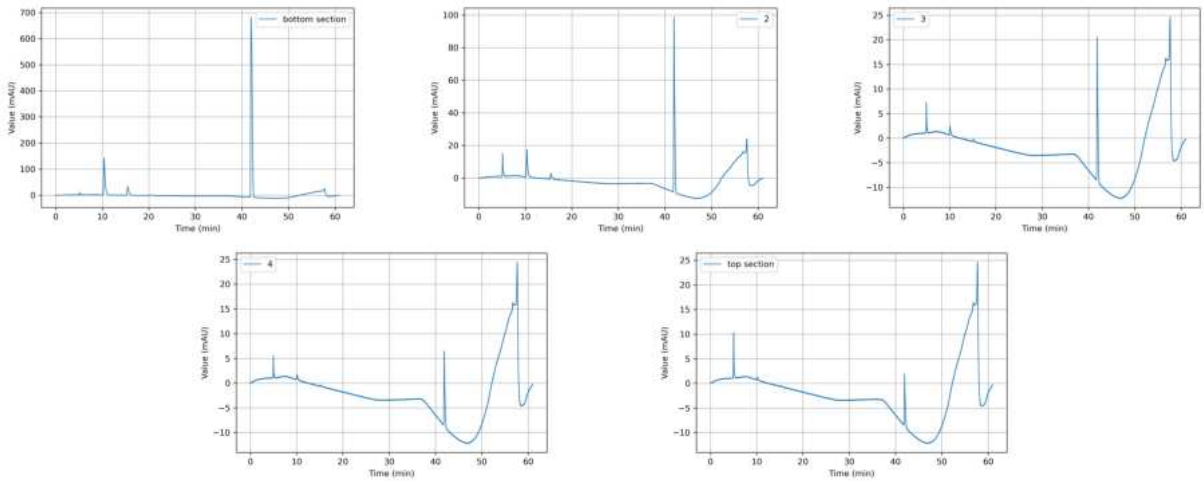

Fig. 33: Chromatograms trap 1

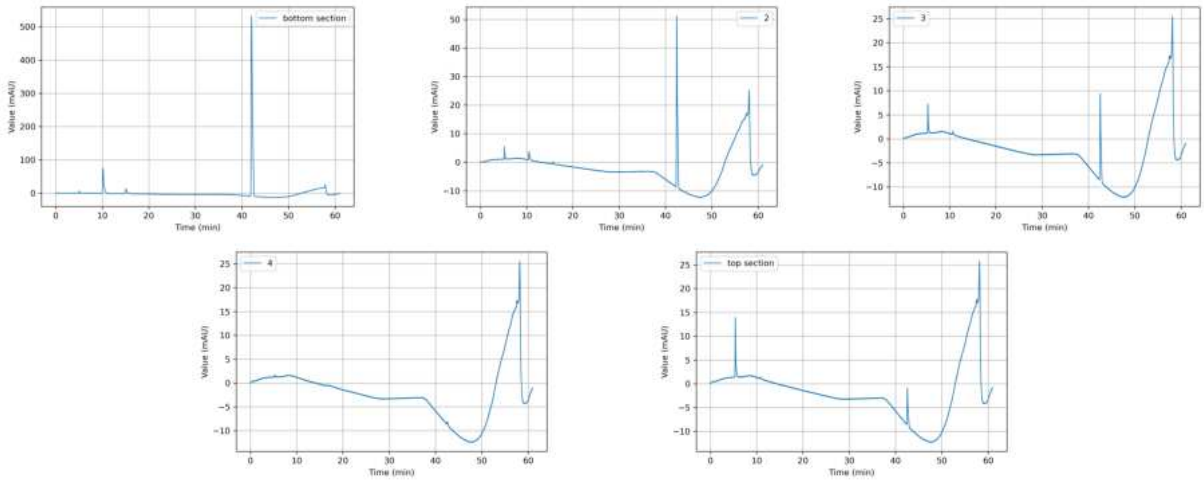

Fig. 34: Chromatograms trap 2

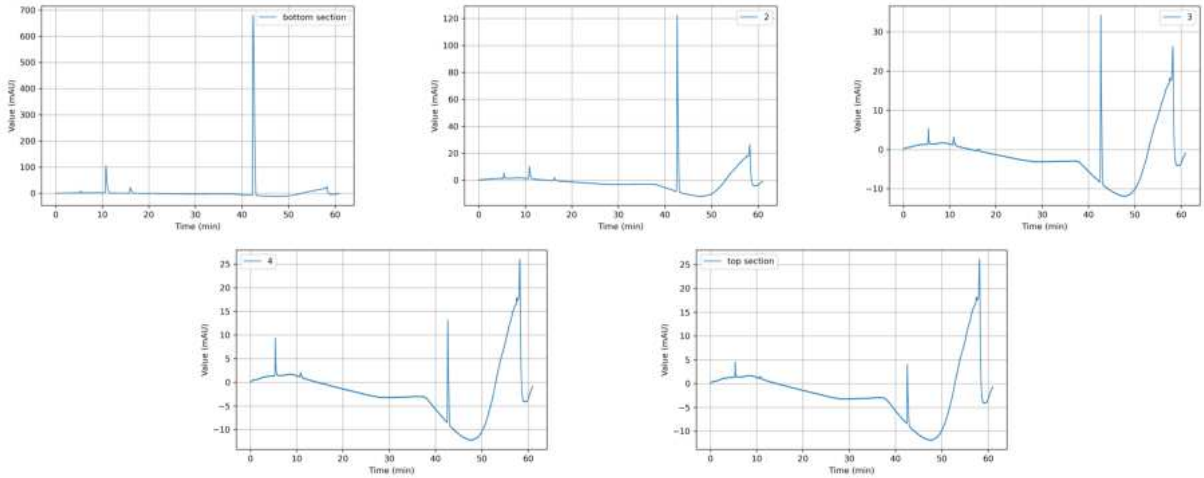

Fig. 35: Chromatograms trap 3

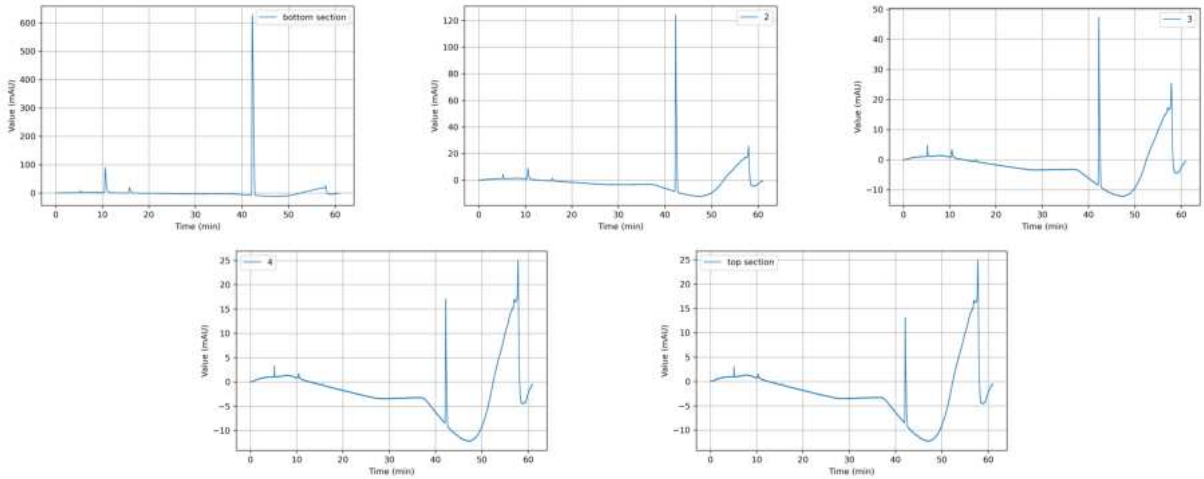

Fig. 36: Chromatograms trap 4

A.2 Data of peak measurements

A.2.1 Aquaeous solution without photosensitizing

Table 3: Data water series: Comparison of undamaged DNA, CPD-dimers, and other damages ((T)6-4(T))

Irrad. time (min)	Retention time (min)	Area (mAU*min)
Undamaged DNA		
1	39.946	28.3725
4	39.698	19.0504
5	39.368	8.7029
6	38.911	8.0167
7	38.694	8.069
8.5	38.643	7.027
10	38.582	6.6639
12.5	38.576	5.5677
15	38.492	5.192
17.5	38.44	4.5516
20	38.419	4.2955
25	38.382	3.2379
CPD-dimers		
1	not av.	0
4	8.045	3.254
5	7.833	6.1244
6	7.55	5.721
7	7.186	4.9969
8.5	7.174	4.9531
10	7.138	6.0614
12.5	7.091	5.7401
15	7.055	6.5916
17.5	7.003	6.3879
20	6.964	5.3151
25	6.95	4.7951
Other damages ((T)6-4(T))		
1	not av.	0
4	12.616	1.0288
5	12.29	1.9382
6	11.879	1.6357
7	11.402	1.3258
8.5	11.368	3.5275
10	11.305	1.0906
12.5	11.302	1.2321
15	11.196	1.2097
17.5	11.13	1.0677
20	11.139	0.934
25	11.084	0.6772

A.2.2 Photosensitization with acetone

Table 4: Data acetone series: Comparison of undamaged DNA, CPD damages and 6-4 damages

Irrad. time (min)	Retention time (min)	Area (mAU*min)
Undamaged DNA		
1	46.681	119.1403
4	46.152	98.4517
8	46.566	60.3031
20	46.377	1.4962
40	46.267	0.1226
60	None	0
90	None	0
CPD damages		
1	14.358	0.4768
4	14.457	7.5055
8	14.393	19.0582
20	14.245	35.5117
40	14.133	32.5917
60	13.983	29.2912
90	13.236	20.4795
6-4 damages		
1	20.362	0.1481
4	20.33	1.9491
8	20.492	5.1454
20	20.294	9.9395
40	20.162	9.3453
60	19.944	8.5122
90	19.04	6.1868

A.2.3 Trap data

Table 5: Data from final study: Enrichment of damaged (CPD), 6-4 damage, and undamaged DNA in the different sections of the thermal traps.

Trap 1						
	CPD		6-4 damage		Undamaged	
Section	Ret Time	Area	Ret Time	Area	Ret Time	Area
1	10.392	45.5246	15.472	12.0496	41.974	245.7643
2	10.344	4.5233	15.491	1.1538	41.945	24.2486
3	10.078	0.4403	15.168	0.1476	41.868	5.9491
4	10.091	0.2321	15.185	0.0715	41.878	3.0724
5	10.136	0.1519	15.228	0.0498	41.956	2.2233

Trap 2						
	CPD		6-4 damage		Undamaged	
Section	Ret Time	Area	Ret Time	Area	Ret Time	Area
1	10.16	21.7056	15.102	5.4254	42.049	178.1903
2	10.51	0.7167	15.704	0.2345	42.422	13.1361
3	10.683	0.1387	15.933	0.0605	42.532	3.763
4	None	None	None	None	42.533	0.1341
5	10.845	0.0666	16.092	0.0197	42.557	1.6818

Trap 3						
	CPD		6-4 damage		Undamaged	
Section	Ret Time	Area	Ret Time	Area	Ret Time	Area
1	10.801	33.3335	16.032	7.9617	42.423	250.974
2	10.895	2.5141	16.225	0.6346	42.643	31.6047
3	10.883	0.4951	16.2	0.1362	42.644	9.5696
4	10.869	0.2024	16.167	0.0704	42.643	4.8339
5	10.847	0.0909	16.116	0.0473	42.545	2.7477

Trap 4						
	CPD		6-4 damage		Undamaged	
Section	Ret Time	Area	Ret Time	Area	Ret Time	Area
1	10.64	27.4832	15.843	6.9631	42.232	221.9673
2	10.549	2.2675	15.785	0.658	42.304	31.8819
3	10.49	0.6294	15.694	0.2134	42.245	12.478
4	10.421	0.1807	15.577	0.0811	42.196	5.5614
5	10.317	0.1689	15.457	0.0699	42.094	4.7019

A.2.4 Enrichement of substances in each thermal trap

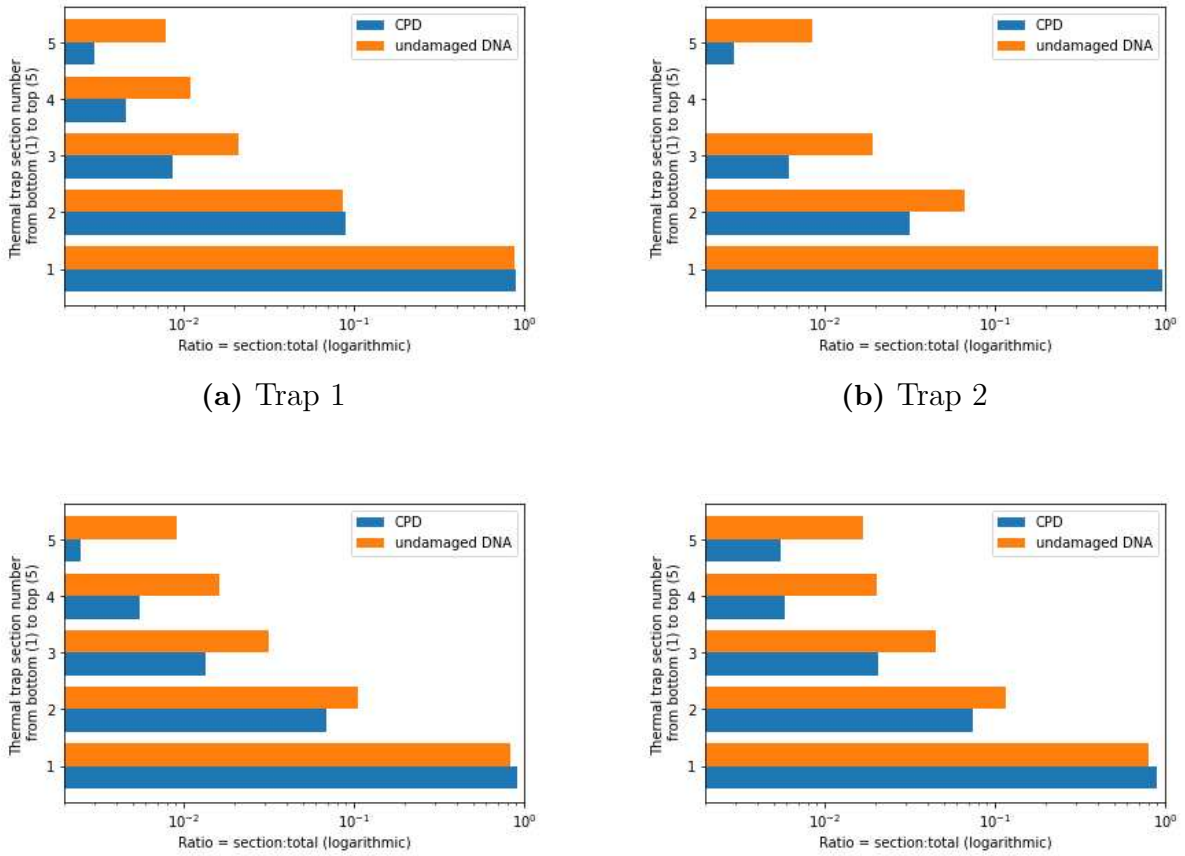

(a) Trap 1

(b) Trap 2

(c) Trap 3

(d) Trap 4

Fig. 37: Ratio of amount of substance found in section to the total amount of substance in each trap: CPD (blue), undamaged DNA (yellow). The x-scale is logarithmic for a better overview of the small values. In the figure the individual distributions are roughly linear, indicating an exponential character.

List of Figures

List of Tables

References

[1] Paula Aikkila. Magnesium and ph gradients in thermal non-equilibrium conditions. Bachelor thesis, Ludwig-Maximilians-Universität, München, 2020.

[2] Adrian Bejan and Khairy R. Khair. Heat and mass transfer by natural convection in porous medium. *International Journal of Heat and Mass Transfer*, 28(5):909–918, 1985.

[3] Jeremy M. Berg, John L Tymoczko, and Lubert Stryer. *Stryer Biochemie*. Springer Spektrum, Heidelberg, Germany, 7th edition, 2014.

[4] Santosh Kumar Bhardwaj, K. Dwivedi, and D.D Agarwal. A review: Hplc method development and validation. *International Journal of Analytical and Bioanalytical Chemistry*, 5(4):76–81, 2015.

[5] S. E. Braslavsky. Glossary of terms used in photochemistry, 3rd edition (iupac recommendations 2006). *Pure and Applied Chemistry*, 79(3):293–465, 2007.

[6] Tom Brown and Dorcas J. S. Brown. Purification of synthetic dna. In *Methods in Enzymology*, volume 211, pages 20–36. Academic Press, San Diego, 1992.

[7] Thierry Douki. The variety of uv-induced pyrimidine dimeric photoproducts in dna as shown by chromatographic quantification methods. *Photochemical & Photobiological Sciences*, 12:1286–1302, 2013.

[8] Thierry Douki, Magali Court, and Jean Cadet. Electrospray–mass spectrometry characterization and measurement of far-uv-induced thymine photoproducts. *Journal of Photochemistry and Photobiology B: Biology*, 54:145–154, 2000.

[9] Stefan Duhr and Dieter Braun. Why molecules move along a temperature gradient. *Proceedings of the National Academy of Sciences (PNAS)*, 103(52):19678–19682, 2006.

[10] Douglas T. Gjerde, Christopher P. Hanna, and David Hornby. *DNA Chromatography*. Wiley-VCH Verlag GmbH & Co. KGaA, Weinheim, 2002.

[11] Remedios González-Luque, Teresa Climent, Israel González-Ramírez, Manuela Merchán, and Luis Serrano-Andrés. Singlet-triplet states interaction regions in dna/rna nucleobase yypersurfaces. *Journal of Chemical Theory and Computation*, 6(7):2103–2114, 2010.

[12] Ivo G. Gut, Paul D. Wood, and Robert W. Redmond. Interaction of triplet photosensitizers with nucleotides and dna in aqueous solution at room temperature. *Journal of the American Chemical Society*, 118(10):2366–2373, 1996.

[13] Hannes Hartmann. *Licht-Materie Wechselwirkung an deponierten Molekülaggregaten und freien Silber-Nanopartikeln.* Dissertation, Universität Rostock, Rostock, Germany, 2016.

[14] Corinna L. Kufner, Dominik B. Bucher, and Dimitar D. Sasselov. The photophysics of nucleic acids: Consequences for the emergence of life. *ChemSystemsChem*, 2022, 2022.

[15] Christof B. Mast, Severin Schink, Ulrich Gerland, and Dieter Braun. Escalation of polymerization in a thermal gradient. *Proceedings of the National Academy of Sciences*, 110(20):8030–8035, 2013.

[16] Thomas Matreux, Paula Aikkila, Bettina Scheu, Dieter Braun, and Christof B. Mast. Heat flows enrich prebiotic building blocks and enhance their reactivity. *Nature*, 628:110–116, April 2024.

[17] Roger L. Miesfeld and Megan M. McEvoy. *Biochemistry.* W. W. Norton & Company, 1st edition, 2017.

[18] Wanmeng Mu, Qingkai Han, Zhaofeng Luo, and Yuzhen Wang. Production of cis-syn thymine-thymine cyclobutane dimer oligonucleotide in the presence of acetone photosensitizer. *Analytical Biochemistry*, 353:117–123, 2006.

[19] Parker, Anthony William, Quinn, and Susan Jane. *Infrared Spectroscopy of DNA*, pages 1065–1074. Springer Berlin Heidelberg, Berlin, Heidelberg, 2013.

[20] Restiani Alia Pratiwi and Asep Bayu Dani Nandiyanto. How to read and interpret uv-vis spectrophotometric results in determining the structure of chemical compounds. *Indonesian Journal of Educational Research and Technology*, 2(1):1–20, 2022.

[21] Jean-Luc Ravanat, Thierry Douki, and Jean Cadet. Direct and indirect effects of uv radiation on dna and its components. *Journal of Photochemistry and Photobiology B: Biology*, 63:88–102, 2001.

[22] Maren Reichl, Mario Herzog, Alexandra Götz, and Dieter Braun. Why charged molecules move across a temperature gradient: The role of electric fields. *Physical Review Letters*, 112(19):198101, 2014.

[23] Maren Reichl, Mario Herzog, Ferdinand Greiss, Manuel Wolff, and Dieter Braun. Understanding the similarity in thermophoresis between single- and double-stranded dna or rna. *Physical Review E*, 91(6):062709, 2015.

[24] Patrick J Rochette, Jean-Philippe Therrien, Regen Drouin, Daniel Perdiz, Nathalie Bastien, Elliot A Drobetsky, and Evelyne Sage. Uva-induced cyclobutane pyrimidine dimers form predominantly at thymine–thymine dipyrimidines and correlate with the mutation spectrum in rodent cells. *Nucleic Acids Research*, 31(11):2786–2794, 2003.

[25] Marin Sapunar, Wolfgang Domcke, and Nadja Došlić. Uv absorption spectra of dna bases in the 350–190 nm range: assignment and state specific analysis of solvation effects. *Physical Chemistry Chemical Physics*, 21:22782–22793, 2019.

[26] Wolfgang J. Schreier, Peter Gilch, and Wolfgang Zinth. Early events of dna photodamage. *Annual Review of Physical Chemistry*, 66:497–519, 2015.

[27] Cynthia Seaver and Paul Sadek. Solvent selection, part i: Uv absorption characteristics. *LCGC*, 12(10):742 – 746, 1994.

[28] Juan José Serrano-Pérez, Israel González-Ramírez, Pedro B. Coto, Manuela Merchán, and Luis Serrano-Andrés. Theoretical insight into the intrinsic ultrafast formation of cyclobutane pyrimidine dimers in uv-irradiated dna: Thymine versus cytosine. *The Journal of Physical Chemistry B*, 112(45):14096–14098, 2008.

[29] Rajeshwar P. Sinha and Donat-P. Häder. Uv-induced dna damage and repair: a review. *Photochemical & Photobiological Sciences*, 1:225–236, 2002.

[30] Agilent Technologies. *Tips and Tricks: HPLC Troubleshooting*, Accessed: 2024-11-20. `https://www.researchgate.net/profile/Avtar-Singh-7/post/What_is_the_reason_behind_negative_peaks_in_HPLC_Chromatogram_for_capsaicin_extract/attachment/59d6412879197b807799d37f/AS%3A433778146451456%401480432177141/download/Tips_and_Tricks_HPLC_Troubleshooting.pdf`.

[31] Thermo Fisher Scientific. Hplc basics. `https://www.thermofisher.com/de/de/home/industrial/chromatography/chromatography-learning-center/liquid-chromatography-information/hplc-basics.html#menu1`, Accessed: 2024-11-20. Accessed: 2024-11-03.

[32] Silvia Tornaletti and Gerd P. Pfeifer. Uv damage and repair mechanisms in mammalian cells. *BioEssays*, 18:221–228, 1996.

[33] A. J. Varghese. Photochemistry of thymidine in ice. *Biochemistry*, 9(24):4781–4787, 1970.

[34] Mark Wainwright. *Photosensitisers in Biomedicine*. John Wiley & Sons Ltd., 2009.

[35] Manuel Wolff. *Thermophoresis of polymers in electrolyte solutions*. Dissertation, Ludwig-Maximilians-Universität, München, January 2016.

[36] Yasuhiro Oba, Toshiki Koga, Yoshinori Takano, et al. Uracil in the carbonaceous asteroid (162173) ryugu. *Nature Communications*, 14(1):1292, 2023.

Declaration of authorship

Hiermit erkläre ich, die vorliegende Arbeit selbständig verfasst zu haben und keine anderen als die in der Arbeit angegebenen Quellen und Hilfsmittel benutzt zu haben.

München, December 5, 2024

Name